November 2015

Quantum Calculations of Aldol Condensation in Acidic Zeolites

Angela N. Migues
University of Massachusetts Amherst

QUANTUM CALCULATIONS OF ALDOL CONDENSATION IN ACIDIC ZEOLITES

A Dissertation Presented

by

ANGELA N. MIGUES

Submitted to the Graduate School of the
University of Massachusetts Amherst in partial fulfillment
of the requirements for the degree of

DOCTOR OF PHILOSOPHY

SEPTEMBER 2015

Chemistry

QUANTUM CALCULATIONS OF ALDOL CONDENSATION IN ACIDIC ZEOLITES

A Dissertation Presented

by

ANGELA N. MIGUES

Approved as to style and content by:

Scott M. Auerbach, Chair

Bret Jackson, Member

S. Thayumanavan, Member

Wei Fan, Member

Craig T. Martin, Department Chair Chemistry

In loving memory of my mother, Karen S. Migues.
Without the enduring memory of your love, I would not have had the fuel to make the journey.

"Heed these words, You who wish to probe the depths of nature: If you do not find within yourself that which you seek, neither will you find it outside. In you is hidden the treasure of treasures. Know Thyself and you will know the Universe and the Gods."

-Oracle of Delphi

ACKNOWLEDGEMENTS

I would like to deeply thank Scott Auerbach for being a wonderful Ph.D. advisor. Scott has always believed in me and during many tough times, knowing this has helped carry me through. Also I would like to thank Scott for being an inspiration to me as an educator and one of the best teachers I have ever had. The lessons I have learned from the example that he set both in the classroom and in the lab will resonate with me deeply for the rest of my life.

I would also like to thank my committee Professors Bret Jackson, Sankaran Thayumanavan and Wei Fan for providing insight into my work and continually challenging me with tough questions. These challenges have only helped to further fuel my love of learning. In addition, I would like to thank Robert Vergenz, my undergraduate research mentor who played integral role in my development as a scientist. My love for computational chemistry began when he gave me an opportunity to do research work in his lab.

I would like to thank past group member Jacob Harvey for continual technical support and for teaching me everything I know about Linux. I would like to especially thank my collaborator, S. Vaitheeswaran, for his continual help and discussions. More importantly, I would like to thank him for his understanding nature. This virtue not only strengthened our professional relationship but also provided the strong foundation of our friendship. I would also like to thank the Northeastern Alliance for Bridging the Gap to the Professorate (NEAGEP) and the National Science Foundation for generous funding opportunities.

I also would like to extend my deepest thanks to all of the friends I have made during my time here in 'The Valley'. Specifically, I would like to thank Meredith, Mikhail, Ashley, John, Kyle and Rose. Throughout the perils of my Ph.D. you all have supported me wholeheartedly. The past five years I've spent here with you have undoubtedly been some of the best years of my life. The lessons I have learned from each of you about friendship I am convinced cannot be found in any book. For this addition to my life, I am truly grateful.

Most importantly, I would like to thank my family. Specifically I'd like to thank my sisters, Erika Migues and Kristin Haskins, for constant love and support throughout my Ph.D. I would like to thank my nephew Caden Haskins. The world as seen through youthful eyes has truly been inspirational to my work. Moreover I would also like to thank my father, Edward Migues. The tenacity I learned from you has served me well throughout my struggles, both in my Ph.D. and in life. Above all others I would like to thank my mother, Karen Migues. Without the virtue of her love, none of this would have ever been possible.

ABSTRACT

QUANTUM CALCULATIONS OF ALDOL CONDENSATION IN ACIDIC ZEOLITES

SEPTEMBER 2015

ANGELA N. MIGUES

B.S., UNIVERSITY OF NORTH FLORIDA

Ph.D., UNIVERSITY OF MASSACHUSETTS AMHERST

Directed by: Professor Scott M. Auerbach

We have used Density Functional Theory to model the mixed aldol condensation reaction catalyzed by acidic zeolites. We have studied the convergence of barriers for the keto-enol tautomerization of acetone in cluster models of HZSM-5 and HY ranging in size from 3-37T. A key finding was that activation barriers for keto-enol tautomerization of acetone in both zeolites (~20 kcal/mol) are significantly higher than those for the condensation reaction between the acetone enol and formaldehyde in 11T cluster models of HZSM-5 and HY. Moreover we found that three zeolite clusters of HZSM-5, similarly sized but including different structural features of the zeolite framework, gave very different activation barriers. These results indicated that a more rigorous approach to constructing cluster models of zeolites was needed.

We have developed two different approaches to build cluster models of zeolites and used two acid-zeolite-catalyzed processes related to the conversion of biomass as platforms to systematically investigate cluster-size convergence. Our central finding is that clusters generated with multi-centered spherical cutoffs yield converged reaction

energies with smaller system sizes than clusters generated by counting framework bonds. The delta approach to constructing finite clusters of zeolite crystals provides a well-defined prescription and employs a single length scale (δ = 5 Å) to converge reaction energies to within chemical accuracy (±1 kcal/mol).

Although reaction energies were convergent at δ = 5 Å, it is not clear that a single length scale is sufficient to converge activation barriers. We used two reaction systems as platforms to establish convergence of activation barriers using delta clusters. We find that a $\delta \geq 4$ Å cutoff is sufficient to converge activation barriers to within chemical accuracy (±1 kcal/mol). After convergence was established, we studied the acid-zeolite-catalyzed mixed aldol condensation of acetone with more biomass-relevant aldehydes, such as hydroxymethyl furfural and furfural, in δ = 4 Å clusters of HZSM-5. We have found that the mechanism for condensation in HZSM-5 is concerted, unlike that of the homogeneous acid catalyzed mechanism. Ultimately, we conclude that the keto/enol tautomerization of acetone remains rate-determining in the case of condensation with formaldehyde, furfural or hydroxymethyl furfural in HZSM-5.

TABLE OF CONTENTS

LIST OF TABLES

Table **Page**

LIST OF FIGURES

Figure **Page**

CHAPTER 1

INTRODUCTION

The dependence of the global economy on petroleum, partnered with limited supply and environmental concerns, have increased the urgency for developing cellulosic biofuels as a renewable, carbon-neutral fuel source[1]. Biomass refinement often begins with conversion of a cellulosic biomass source to oxygenated intermediates, which can then be catalytically processed to yield biofuels or biomass-based chemicals[2-4]. Although progress has been made in streamlining these processes, many production methods remain too inefficient or environmentally unfriendly for wide-scale substitution of petroleum. The mixed aldol condensation represents an example of such a process for upgrading biomass-derived species. This reaction forms a new carbon-carbon bond between, e.g., acetone and formaldehyde (Fig. 1.1), effectively lengthening the hydrocarbon chain by joining together smaller, molecular components. Ultimately converting smaller oxygenates to larger feedstocks suitable for producing fuels and chemicals.

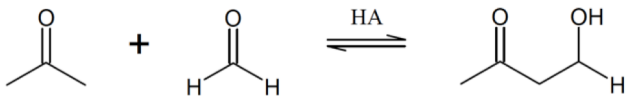

Figure 1.1: The acid-catalyzed aldol reaction between acetone and formaldehyde (HA is a general acid catalyst).

The complete homogeneous acid-catalyzed1mixed aldol condensation actually consists of three steps: (*i*) keto/enol tautomerization, (*ii*) condensation between the enol and aldehyde, and (*iii*) elimination of water to yield an olefin[5-7]. Throughout our work,

we refer to the first step as ‘tautomerization’ and the second as ‘condensation.’ Since we focus on carbon carbon bond formation, we do not consider the third step. The reaction including steps one and two is referred to throughout as the mixed aldol condensation.

The homogeneous acid-catalyzed keto-enol tautomerization mechanism begins with the rate-determining tautomerization step, followed by condensation to form the new carbon-carbon bond[1,4] (see Fig. 1.2) . Homogeneous acid catalysis, using corrosive solutions, lacks product selectivity and produces environmentally hazardous chemical waste. Growing concerns about the environmental impacts of such caustic solvents has sparked a movement toward more green heterogeneous catalysts. In recent years, due to their tunable acid sites and controllable properties, zeolites have emerged as promising solid catalysts for aldol condensation reactions[1,4]. Running aldol condensations in nanoporous catalysts such as acidic zeolites can both mitigate the costs and environmental impacts of large-scale acidic/caustic processing,[1,4] and may confer new and useful selectivities over product formation[8-10].

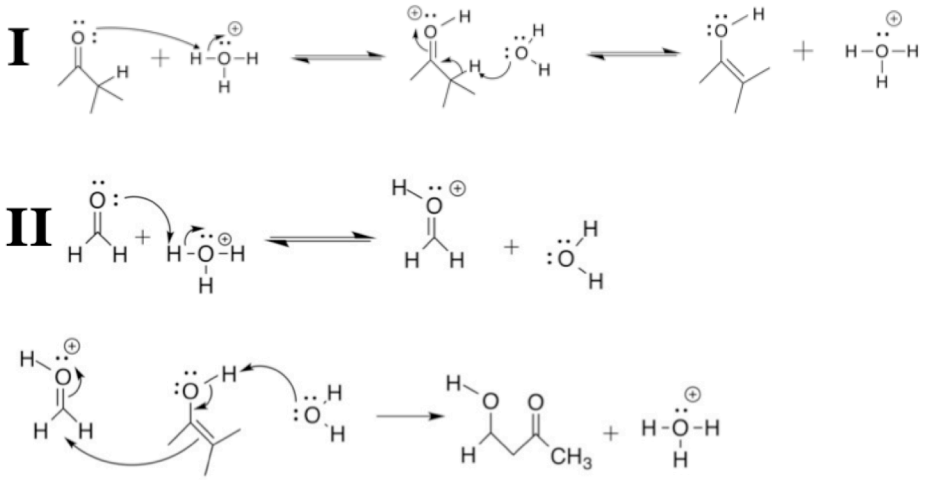

Figure 1.2: Reaction mechanism for the liquid phase, acid-catalyzed aldol reaction between acetone and formaldehyde. The first step is the keto-enol tautomerization of acetone (I) and the second step (II) is carbon-carbon bond formation.

Zeolites are microporous, alumino-silicates composed of TO_4 (T = Si or Al) subunits, which form larger 3-dimensional structures consisting of channels, intersections, and cages[11]. Several properties of zeolites distinguish them from other solid catalysts; these include the molecular-sized dimensions of the pores, the strong Brønsted acid sites, and the hydrothermal stabilities allowing relatively facile catalyst regeneration[11,12]. The polar nature of the Si-O bond and the presence of charges in some zeolites can impose relatively strong electric fields on adsorbed guests and as such, confinement of guest molecules within zeolite pores can perturb guest electronic structures and constrain reactive geometries, hence influencing (increasing or decreasing) rates for reaction paths that occur outside the zeolite[8,10,12,13]. However, it remains unclear whether confinement in zeolite nanopores alters the conventional mechanism of aldol condensation and if the second step of acid-catalyzed aldol condensation – the bimolecular combination step – can proceed rapidly in such a restricted space. We hypothesize that in the confined space of the zeolite pore, the condensation step will become rate-determining once the size of the guest molecules approaches the size of the pore.

In our work we will focus on this issue. It is our objective to address the following key questions:

- How do acid zeolites catalyze aldol condensation reactions?
- How does the mechanism change?
- How do acid zeolites with different pore structures catalyze these processes?
- How are barriers affected as the size of the guest molecule approaches the

size of the zeolite pore?

Relatively few computational studies of zeolite catalysis have investigated aldol chemistry, and these have focused on the tautomerization step[5-6]. For example, computational work by Boekfa *et al*.[5] on acetone tautomerization in acid zeolites HFER, HZSM-5, and HMCM-22 suggests that relative strengths of host-guest hydrogen-bonding interactions with Brønsted acid sites at reactant (adsorbed acetone) and transition state are critical for determining activation energies. Tautomerization activation energies and endothermic reaction energies were found to increase with decreasing zeolite pore size, as smaller pores perturb host-guest hydrogen bonding[5]. However, in the study by Boekfa *et al.* the condensation step was not investigated, and only a few zeolite atoms were allowed to relax. Also, though Boekfa *et al.* performed calculations on relatively large ("34T") zeolite clusters, there was no study of convergence with respect to system size, leaving open the question of an optimal cluster size for future calculations.

We employ finite cluster models of zeolite crystals to investigate the energetics underlying aldol condensation in acidic zeolites. Several alternative computational methods exist for treating long-range zeolite-guest interactions. Periodic density functional theory (DFT) codes such as VASP[14] have proven useful for zeolites with small unit cells[15-17], but calculations quickly become intractable for larger zeolites with, e.g., FAU (e.g., zeolite HY) or MFI (HZSM-5) structure types.[18] The QM-Pot approach[19-20] reported by Sauer and coworkers treats long-range interactions efficiently by mixing quantum and molecular mechanics (MM) calculations,[21-22] although this approach often relies on using DFT to parameterize the MM portion, which can be a cumbersome process. Other approaches for mixing quantum mechanics and force field calculations,

generally denoted as QM/MM methods, have been applied to study reactions in zeolites.[23-26] However, QM/MM approaches may exhibit numerical instabilities when computing transition states,[27] potentially limiting their usefulness. In contrast, cluster calculations are relatively simple to apply to a wide range of zeolites[28].

As such, finite cluster models of zeolite crystals have been extensively employed to understand reactive and adsorptive processes in zeolites of various framework types.[29] Convergence with respect to zeolite cluster size is possible despite the presence of long-range interactions, because the slowly varying, long-range contributions to reaction and activation energies—energy differences between nearby configurations—essentially cancel for large enough but finite cluster sizes[30]. It is not obvious, however, how large zeolite clusters need to be for such cancellation to occur.

The above concerns suggest the following questions:

- How do we construct finite cluster models of zeolite crystals that properly capture the essential chemistry?
- How big is 'big enough'?

Below we describe the results of our work. First we present our work modeling mixed aldol condensations in acid zeolites, HZSM-5 and HY. Here we investigate the energetics underlying aldol condensation for medium- and large-pore zeolites HZSM-5 and HY, respectively, to determine if pore size alters the conventional mechanism of aldol condensation. We focus on converging activation barriers for the keto-enol tautomerization of acetone with respect to cluster size of HY and HZSM-5, finding different convergence properties for the two zeolites. Ultimately, we will show that the keto-enol tautomerization of acetone is rate-determining in the overall condensation

reaction with formaldehyde in HZSM-5 and HY. Next we performed systematic computational tests on zeolite cluster models in search of simple rules that govern system-size convergence of zeolite-guest interactions. We will show that our approach to building cluster models of zeolite crystals provides a well-defined prescription for constructing finite cluster models of zeolites and requires a single length scale. Next, we will locate transition states for the mixed aldol condensation reaction in cluster models of HZSM-5 constructed according to the delta approach. We will show that activation barriers for both keto-enol tautomerization of acetone and subsequent condensation with formaldehyde converge with respect to increasing cluster size. Lastly, we will present our results modeling the condensation step with more biomass-relevant aldehydes, furfural and hydroxymethyl furfural (HMF). We will show that, unlike homogenous acid catalysis, the condensation mechanism in HZSM-5 is concerted. Ultimately, we will show that keto-enol tautomerization of acetone remains rate-determining in the condensation reaction with all aldehydes studied.

CHAPTER 2

DENSTIY FUNCTIONAL THEORY STUDY OF MIXED ALDOL CONDENSATION CATALYZED BY ACIDIC ZEOLITES HZSM-5 AND HY

2.1 Introduction

In the present study we applied clusters to model the aldol condensation of acetone and formaldehyde catalyzed by zeolites HZSM-5 and HY, important examples of medium- and large-pore zeolites. Although biomass-derived aldehydes such as furfural are more industrially relevant[8], our study of formaldehyde condensation with acetone establishes key methodological parameters for our future computational study of furfural condensation. Our calculations below on both zeolites corroborate the homogeneous-phase mechanism, involving slow keto/enol tautomerization and fast condensation. We thus seek to converge the keto/enol activation energy for both acid zeolites with respect to cluster size. We note that such convergence is possible despite the presence of long-range contributions to host-guest interactions. This is because when computing activation energies – energy differences between nearby configurations – the slowly varying, long-range contributions essentially cancel for large enough but finite cluster sizes[30]. The question remains whether HY and HZSM-5 keto/enol barriers converge at similar cluster sizes. We address this below, finding that HY barriers converge faster than those of HZSM-5. The system-size study of barriers in HZSM-5 reported below suggests two regimes: a small-to-medium cluster regime, possibly mimicking catalysis at Brønsted acid sites on external surfaces of an HZSM-5 crystallite, and a medium-to-large cluster regime capturing intracrystalline catalysis. This intracrystalline regime was found to emerge only after Brønsted acid-site partial charges reach plateau values, suggesting a

new approach for establishing convergence with respect to zeolite cluster size.

2.2 Methods

2.2.1 Zeolite Models

In this study, we used cluster methods to model the acid-catalyzed aldol condensation between acetone and formaldehyde in HZSM-5 and HY clusters of various sizes. In general, we specify cluster size by indicating the number of tetrahedral atoms (Si or Al) in a given cluster. For example, an "11T" cluster contains one Al atom and ten Si atoms (in addition to several oxygens and hydrogens). The designation 11T does not give the precise atom count, connectivity, or three-dimensional structure of a cluster). Rather, the notation 11T gives a rough sense of cluster size compared to, e.g., 20T or 37T.

We don't use QM/MM embedded cluster methods below because of numerical instabilities we have encountered during transition state searches with such embedded clusters[27]. Nor do we use periodic plane wave approaches because of the very large unit cells in HZSM-5 ("MFI" structure type) and HY ("FAU" structure type) zeolites[18]. Instead, we apply the medium-sized clusters shown in Fig. 2.1A (HZSM-5) and Fig. 2.1B (HY) to efficiently investigate the relative energetics of the tautomerization and condensation kinetics in both zeolites. Such clusters capture approximately half the HZSM-5 pore intersection and the HY supercage, and may be viewed as providing rough models of Brønsted acid site catalysis on external zeolite surfaces. We performed a cluster-size convergence study using clusters in the range 3T-37T for both zeolites. Such a study allows comparison of system-size convergence between HY and HZSM-5, and investigation of the role of "completing a pore" versus converging electronic properties such as acid-site charge.

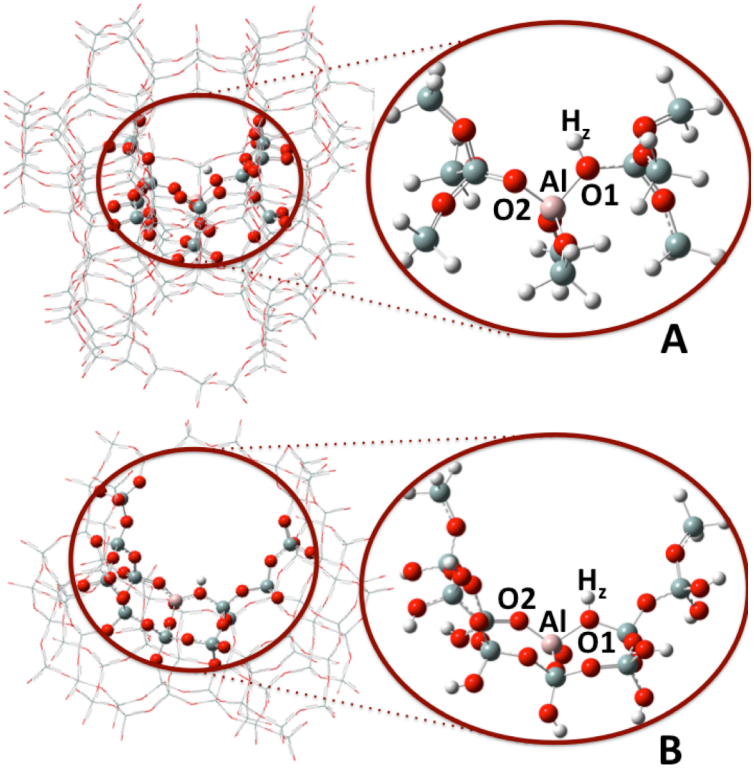

Figure 2.1: (A) HZSM-5 zeolite cluster and (B) HY zeolite cluster, where the 11T cluster is shown as ball and stick with the extended framework as wire mesh; the 11T cluster used shown inset, where oxygen numbers are defined for consistency with those in HY. For comparison between active sites in HY and HZSM-5, we denote the two active oxygens as O1 and O2 in both structures; these are not the crystallographically-sanctioned labels in HZSM-5.

Zeolite clusters used in this study were extracted from the X-ray crystallographic data of Czjzek *et al*.[31] for HY, and of van Koningsveld *et al*. for HZSM-5[32]. Here we employ the common nomenclature that zeolite rings with *n* T-atoms are denoted *n*-rings. The HY framework structure is comprised of a tetrahedral network of roughly spherical cages, each connected to four adjacent cages through 12-ring windows of nominal diameter ~7.4 Å[18]. In contrast, HZSM-5 features 10-ring channels running along the crystallographic *b*-axis, which intersect with 10-ring sinusoidal channels running along the *a*-axis, all of which exhibit a diameter of about 5.5 Å[18]. The cluster models of HZSM-5 were all constructed at the intersection of the 10-ring straight and sinusoidal channels, and were built around the Brønsted acid site between Si(2) and Si(8), centered on O(13) (see Fig. 2.1A)[23]. Due to its proximity to the intersection, O(13) is a catalytically relevant site[23]. The HY cluster models were centered on O(1) in the 12-ring window with the Brønsted acid site pointed directly into the supercage (see Fig. 2.1B). The applicability of the O(1) site as the Brønsted acid site was previously determined to be a catalytically relevant position[30]. We note in Figs. 2.1A and 2.1B that the two active oxygens, O(13) and O(1) in HZSM-5 and HY respectively, are denoted as O1 in both structures for ease of comparison between active sites in HY and HZSM-5; these are not the crystallographically-sanctioned labels.

In general we seek to terminate all zeolite clusters with fixed OH groups to mimic the electronic environment of zeolites. However, doing so may introduce strong steric effects between capping hydrogens. We found such steric overlaps, e.g., in the 11T HZSM-5 cluster shown in Fig. 2.1A. The 11T HZSM-5 cluster model shown in Fig. 2.1A was thus terminated at silicon atoms with capping hydrogens placed along the vector

towards nearest-neighbor oxygens at an Si-H bond distance of 1.4 Å and subsequently frozen. In the 11T HY cluster, shown in Fig. 2.1B, terminal framework oxygens were capped with hydrogens, placed in the location of the next framework silicon atom at an O-H bond distance of 0.9 Å and subsequently frozen. In HY the two silicon atoms at the top of the 12-ring window were 'capped' with hydrogens instead of hydroxyl subunits to minimize spurious hydrogen bonding at the edge of the cluster. Restraining terminal atoms mimics the covalent footprint of the zeolite framework structures.

Our cluster convergence study involved the following cluster sizes for HZSM-5 and HY:

- HZSM-5 (11 clusters): 3T, 5T, 9T, 11T, 15T, 20T, 20T′, 21T, 26T, 30T, 37T
- HY (9 clusters): 3T, 5T, 7T, 9T, 11T, 13T, 15T, 20T, 30T.

We note that three similarly-sized cluster models of HZSM-5, shown in Figure 2.2, have been expanded differently around the same Brønsted acid site. In the first cluster model (denoted I) the 10-ring window belonging to the straight channel has been completed and parts of the extended straight channel are included, comprising 20T total size. In the second (II) the 10-ring from the sinusoidal channel has been completed and augmented further with three 5-rings, giving a total size of 21T. The third cluster (III) represents the intersection of straight and sinusoidal channels, in which both 10-ring windows are completed to comprise a 20T cluster size. These three clusters turn out to play an important role in the transition of keto/enol barriers from a small-to-medium plateau regime, to a medium-to-large intracrystalline regime.

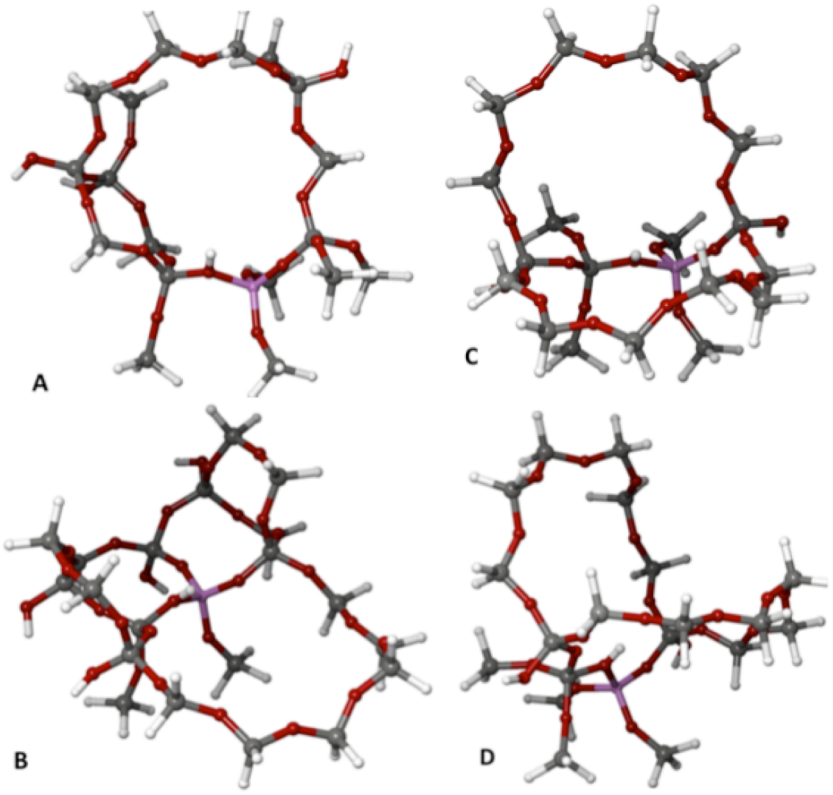

Figure 2.2: Three HZSM-5 cluster models of similar size. A) cluster I is a 20T model of the 10-ring straight channel; B) cluster II is a 21T model of the 10-ring sinusoidal channel with added pentasil rings; C) cluster III is a 20T construction of two 10-rings at the intersection of straight and sinusoidal channels (looking down straight channel); D) side view of cluster III. Images rendered using Maestro[33].

2.2.2 Computational Details

The B3LYP hybrid density functional was used with the 6-311G(d,p) basis set as implemented with the Gaussian09[34] suite in all calculations presented herein[35,36]. This model chemistry has been previously shown by Fermann *et al.*[30] to capture ~90% of activation barriers for proton transfer processes in zeolites. We thus expect similar performance in describing acid-catalyzed aldol chemistry. Dispersion corrections using the Grimme[37] approach, as implemented in the Jaguar[38] computational chemistry software suite, were applied to all structures (reported in Section 2.3.4); these were not found to qualitatively influence the computed trends, likely because of the importance of site-specific hydrogen-bonding in zeolite-catalyzed aldol chemistry. Atomic charges were calculated using the Merz-Kollman procedure to reproduce the electrostatic potential[39,40]. When optimizing geometries and searching for transition states, all atoms in the zeolite clusters were allowed to relax except for terminal "capping" hydrogens on either silicon (HZSM-5) or oxygen (HY) atoms, which were fixed.

To reduce computational cost a semi-empirical, PM6[41], approach was used to quickly explore plausible transition state conformations. Prior to locating all transition states a constrained optimization was performed, in which atoms thought to be involved in the reaction coordinate were frozen, allowing the remaining atoms to relax. Previous computational work on keto/enol acetone tautomerization[5] suggested likely reaction coordinates for this step. In particular, the zeolite protonates the acetone carbonyl while the methyl group donates a proton. As such the acetone carbonyl oxygen, methyl carbon, the two involved protons and the zeolite O1 and O2 atoms (see Fig. 2.1 for oxygen labels) were frozen at various configurations along a likely reaction coordinate, yielding different initial conditions for full transition state searches. For the second step, our

previous experience and chemical intuition suggested that the enol would react with the adsorbed formaldehyde at a carbon-carbon distance of about ~2.6 Å, forming the new carbon-carbon bond while simultaneously donating a proton (from acetone to the zeolite) and accepting a proton (from the zeolite to the formaldehyde carbonyl).

These constrained optimizations were followed by unconstrained transition state searches. All transition states were located using the Berny Optimization algorithm[42], confirmed as first order saddle points by normal mode analysis (NMA), and by steepest-descent calculations to confirm that transition states connect with desired reactant and product minima. NMA was performed on all minima to confirm that they are true minima with all real vibrational frequencies. Confirmed transition states were then used as initial transition state geometries in higher-level calculations using B3LYP. Once found in a given smaller cluster, the corresponding transition state structures were then used as initial geometries in larger cluster sizes. Energetics corrected by zero-point vibrational energy and free energy corrections are provided in the Section 2.3.4; these corrections were not found to change any of the computed trends.

2.3 Results and Discussion

Here we report our results for the mixed aldol condensation reaction between acetone and formaldehyde in three main parts. In Sec. 2.3.1, we report the step-wise, gas-phase (uncatalyzed) mixed aldol condensation; Sec. 2.3.2 details the acid zeolite-catalyzed mixed aldol condensation in 11T models of HZSM-5 and HY; and Sec. 2.3.3 describes the convergence of keto/enol tautomerization barriers with respect to cluster size, with analysis of acid-site atomic charges to rationalize the cluster-size dependence

of activation energies.

2.3.1 Gas-Phase, Uncatalyzed Mixed Aldol Condensation

The gas-phase tautomerization of acetone, having been previously investigated computationally,[5] is used herein to establish the applicability of our model chemistry, and to provide a baseline for understanding the catalytic chemistry. A concerted mechanism for enol formation has been previously established[5, 43-45 46] and hypothesized to be the rate-determining step in the overall reaction[6].

Figure 2.3 shows the potential energy diagram for the gas-phase tautomerization of acetone. The B3LYP/6-311G(d,p) activation energy is 68.2 kcal/mol and the reaction energy is 12.7 kcal/mol. These results agree well with the previously calculated activation and reaction energies computed by Boekfa *et al*.[5] of 68.0 and 9.9 kcal/mol, respectively, using the M06-2X functional[47-48]. Our results also agree well with energies computed using 2nd order Möller-Plesset perturbation theory with 6-31G**//cc-pvtz and 6-31G** basis sets,[45,46] which give activation energies of 64.0 and 69.2 kcal/mol, respectively, and reaction energies of 11.6 and 13.1 kcal/mol. Moreover, the calculated reaction energy is in reasonable agreement with the experimental gas-phase enthalpy of 10 ± 2 kcal/mol, measured by gas phase ionization of suitable precursors[45,46].

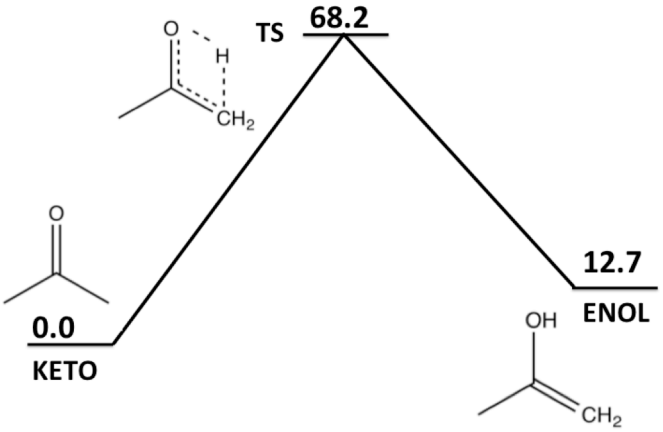

Figure 2.3: Bare electronic energy profile (kcal/mol) and the molecular structure of the gas phase, uncatalyzed tautomerization of acetone.. Reactant state (acetone), transition state and product state (acetone enol) are illustrated above.

Figure 2.4 shows the potential energy diagram for the gas-phase condensation between the acetone enol and formaldehyde. The activation energy is calculated to be 15.0 kcal/mol, with a reaction energy of –22.0 kcal/mol. The gas-phase barrier for condensation is significantly less than that for tautomerization, consistent with the notion that tautomerization is the rate-determining step in the gas phase.

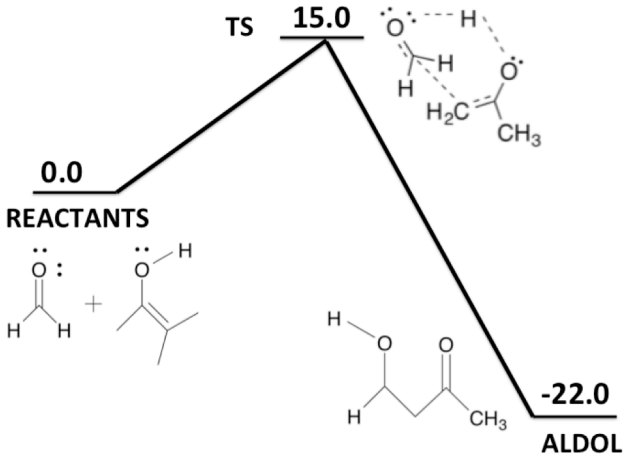

Figure 2.4: Bare electronic energy profile (kcal/mol) and the molecular structure of the gas phase, uncatalyzed condensation between acetone enol and formaldehyde. Reactant state (acetone enol and formaldehyde), transition state and product state (aldol) are illustrated above.

2.3.2 Mixed Aldol Condensation Catalyzed by Acid Zeolites

Next we discuss the mixed aldol condensation catalyzed by acid zeolites HZSM-5 and HY in 11T cluster models. In both zeolites mixed aldol condensation begins with the adsorption and subsequent tautomerization of acetone at the Brønsted acid site. Boekfa *et al*. has previously modeled acetone tautomerization in HZSM-5 using cluster methods[5].

2.3.2.1 Tautomerization Catalyzed by HZSM-5 and HY

Figures 2.5A and 2.5B show potential energy diagrams for the tautomerization of acetone in HZSM-5 and HY, respectively. The activation energies in 11T cluster models of HZSM-5 and HY are 28.1 and 19.3 kcal/mol, respectively. These results are consistent with the trend found by Boekfa *et al*. of decreasing activation energy with increasing pore size[5]. However, our computed activation energy in the 11T cluster model of HZSM-5 is significantly higher than the value of 20.5 kcal/mol calculated by Boekfa *et al*. using a 34T cluster[5]. The convergence of activation energies with respect to cluster size will be discussed in detail in the next section.

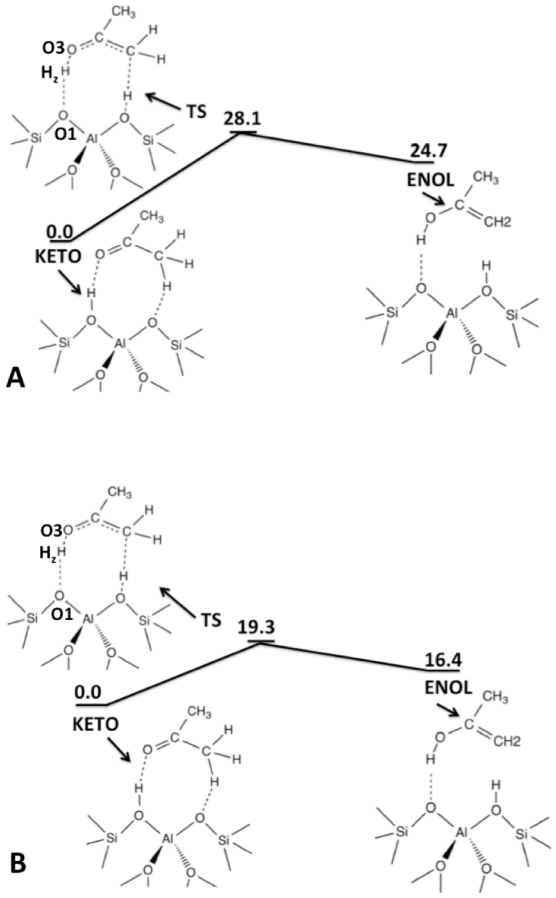

Figure 2.5: Bare electronic energy profile (kcal/mol) and molecular structures for the tautomerization of acetone in an 11T cluster model of HZSM-5 (A) and HY (B) obtained at the B3LYP/6-311G(d,p) model chemistry. Reactant state (acetone), transition state and product (acetone enol) are shown in both.

We wish to be careful not to over-interpret geometrical details of these 11T calculations because of the relatively small size of these clusters. However, in the cluster convergence study detailed in the next section, we find that the 11T HY cluster is essentially converged with respect to system size, while the 11T HZSM-5 cluster is characteristic of a plateau regime that may mimic catalysis on external HZSM-5 surfaces. As such, we seek to understand key differences in HY and HZSM-5 geometric and electronic structures in these 11T clusters.

The tautomerization barriers from our 11T cluster models are controlled by relative strengths of hydrogen bonding at the Brønsted acid site. In HY the barrier is lower than in HZSM-5 due to stronger hydrogen bonding at the Brønsted acid site in the HY transition state. To understand the origin of this hydrogen bonding difference we consider distances, angles, and charges. In particular, the intermolecular $O(3)H_z\cdots O(1)$ distances (see. 2.5 for atom labels) at the transition states are similar in both HY and HZSM-5, while the $O(3)\text{-}H_z\cdots O(1)$ complex is slightly more linear in the 11T model of HY (168.3°) than it is in HZSM-5 (163.2°). As such, the HY $O(3)H_z\cdots O(1)$ hydrogen bond may be somewhat less sterically hindered than it is in HZSM-5. Perhaps more important is the acid-site charge, which correlates with hydrogen-bonding strength. We have computed acid-site charge in the bare zeolite 11T cluster models by summing the ESP charges from O2-Al-O1-H_z atoms (see labels in Fig. 2.1), finding active-site charges of +0.17 in HZSM-5 and +0.34 in HY, correlating with a lower barrier in HY. In the next section we expand our analysis of active site charge as it relates to convergence with respect to cluster size.

The data in Figs. 2.5A and 2.5B also show that the tautomerization reaction is

less endothermic in the 11T model of HY compared to the 11T HZSM-5 cluster, because of stronger hydrogen bonding of the adsorbed enol in HY. The enol in HY exhibits an O(1)···H_z distance of 1.78 Å (see Fig. 2.5 for atom labels) and an O(1)···H_z-O(3) angle of 164.9°, as compared to 2.55 Å and 128.5° in HZSM-5. These findings suggest that subtle differences in zeolite cluster models can produce significant differences in host/guest hydrogen bonding properties.

2.3.2.2 Condensation Catalyzed by HZSM-5 and HY

After acetone tautomerization produces the activated enol, a new carbon-carbon bond forms in the condensation reaction with formaldehyde. The zeolite-catalyzed reaction begins with co-adsorption of the reactant pair in the zeolite framework. The potential energy diagrams for condensation catalyzed by HZSM-5 and HY are shown in Figs. 2.6A and 2.6B, respectively.

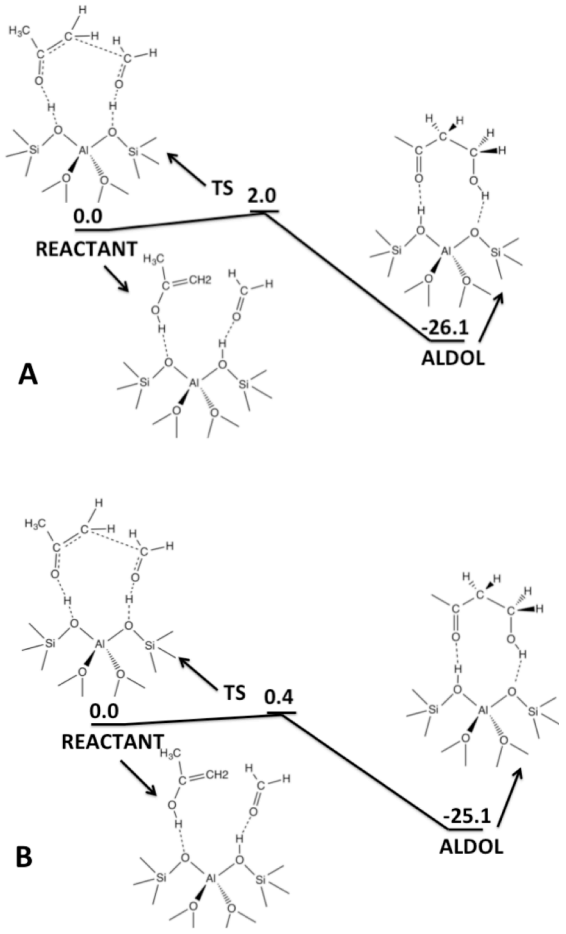

Figure 2.6: Bare electronic energy profile (kcal/mol) and molecular structures for the condensation between the acetone enol and formaldehyde in an 11T cluster model of HZSM-5 (A) and HY (B) obtained at the B3LYP/6-311G(d,p) model chemistry. Reactant pair (acetone enol and formaldehyde), transition state and product (aldol) are shown in both.

The activation energies in these 11T cluster models of HZSM-5 and HY are 2.0 kcal/mol and 0.4 kcal/mol, respectively. The condensation barriers in HZSM-5 and HY are thus significantly lower than those for the uncatalyzed, gas-phase condensation, and also substantially smaller than the barriers for zeolite-catalyzed tautomerization. These 11T cluster models suggest that acetone tautomerization remains the rate-determining step of acetone/formaldehyde mixed aldol condensation even in zeolite pores. Because of the substantial difference in these tautomerization and condensation barriers, we find it extremely unlikely that this conclusion will change for larger clusters. We note that considering zeolite catalysis of mixed aldol condensation between larger guest molecules such as the more industrially relevant acetone/furfural may change this mechanistic picture; we will report on this in Chapter 4. We now proceed to study the convergence of acetone tautomerization barriers with respect to cluster size.

2.3.3 Cluster Size Convergence of Acetone Tautomerization in HZSM-5 and HY

Conventional wisdom in zeolite cluster modeling suggests that completing a pore surrounding a given active site is sufficient to capture the effect of guest molecule confinement. To test this assumption, we investigate the dependence of acetone tautomerization barriers on HZSM-5 and HY cluster sizes. The previously computed acetone tautomerization barrier in HZSM-5 of 20.5 kcal/mol, obtained by Boekfa *et al*. with a relatively large cluster model (34T), serves as a comparison point for our HZSM-5 study[5]. Figure 2.7 shows the dependence of the acetone tautomerization barriers with respect to increasing cluster size in both HZSM-5 and HY zeolites. The activation energies in HZSM-5 and HY exhibit different dependencies on system size. In particular,

convergence in HY is achieved at smaller system sizes (9T-11T) compared to HZSM-5 (26T), where larger clusters were found to be necessary to establish convergence.

In HY activation energies converge rapidly to ~19 kcal/mol for cluster sizes in the range 9T-11T. To our knowledge, activation energies for acetone tautomerization in HY have not been determined, neither experimentally nor theoretically. However our computed activation energy compares well to the value obtained in zeolite MCM-22,[5] which contains 12-rings as does HY. In contrast, for HZSM-5 we found two distinct regimes in Fig. 2.7, involving clusters larger or smaller than ~20T. For HZSM-5 clusters larger than 20T, acetone tautomerization barriers converge to 20.5 kcal/mol, which agrees essentially perfectly with the previously determined value from Boekfa *et al*. [5] For HZSM-5 clusters smaller than 20T, we observe in Fig. 2.7 a broad plateau of barriers at the significantly higher value of ~27 kcal/mol. The stability of this broad plateau region suggests the possibility that this regime is chemically relevant, e.g., to catalysis on HZSM-5 external surfaces. We will investigate this possibility in future work.

Figure 2.7 also shows that there are three similarly sized HZSM-5 clusters connecting these two regimes, with activation energies spanning the range of ~20-28 kcal/mol. Although these clusters are similar in size, they are structurally distinct in that each has been expanded about the Brønsted acid site in a different manner (see Fig. 2.2). We recall that cluster I includes a 10-ring from the straight channel; cluster II comprises a 10-ring from the sinusoidal channel with additional pentasil rings; and cluster III involves the intersection of the two 10-rings.

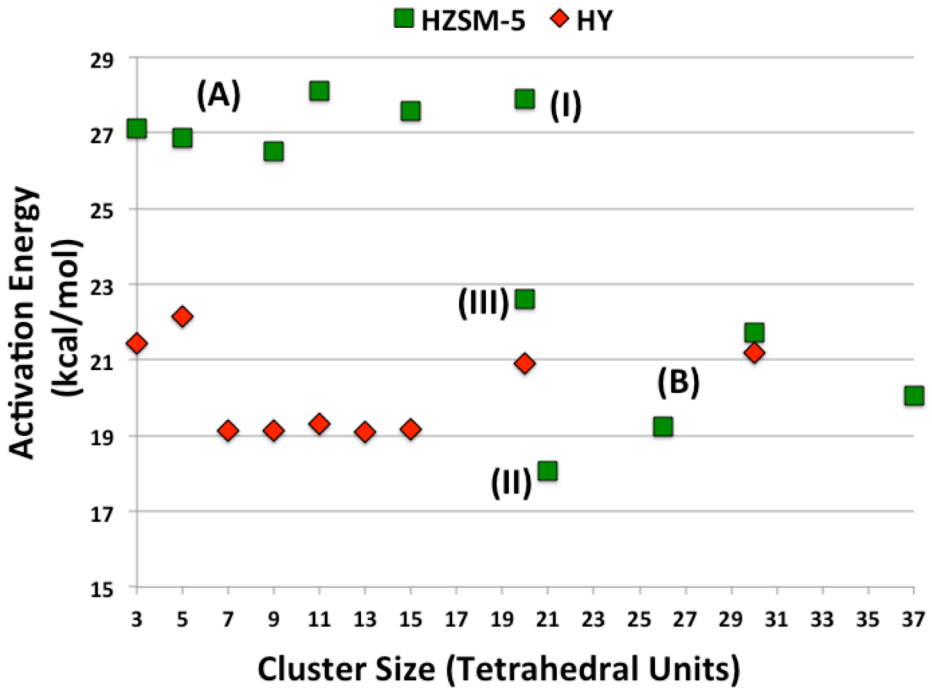

Figure 2.7: The dependence of keto/enol tautomerization bare electronic activation energy with respect to system size in both HZSM-5 and HY zeolites. Two distinct regimes in HZSM-5 are labeled A & B.

The activation energy from cluster I agrees with the 11T cluster model, demonstrating that completion of a 10-ring surrounding an active site in HZSM-5 may be insufficient to converge reaction barriers. The barrier from cluster III agrees well with those from larger clusters such as 30T and 37T, making cluster III the smallest cluster representing the intracrystalline regime. These results beg the following question: which system property governs barriers in cluster models of zeolites? Our analysis of the 11T clusters above suggests that active-site charge is a key property to consider.

Figure 2.8 shows the dependence of total active-site charge with respect to (A) system size and (B) activation energies, in both HZSM-5 and HY. The total charge was obtained by summing ESP charges of individual atoms in the active sites (O2-Al-O1-H_z) of the bare zeolites without guest molecules. In HZSM-5, the total charge on the active site becomes increasingly positive with respect to increasing cluster size (Fig. 2.8A), with a step increase for the critical clusters I, II, and III discussed above. Figure 2.8 also shows that as positive charge accumulates on the HZSM-5 active site, activation energies decrease (Fig. 2.8B) because of increasing host-guest hydrogen-bond strength. I.e., the charge of the active site is directly related to its acidity and thus to the strength of hydrogen bonding between the guest and Brønsted acid site. In HY a different trend is observed; active-site charge very weakly decreases with increasing cluster size (Fig. 2.8B), with no discernable correlation to activation barriers (Fig. 2.8B).

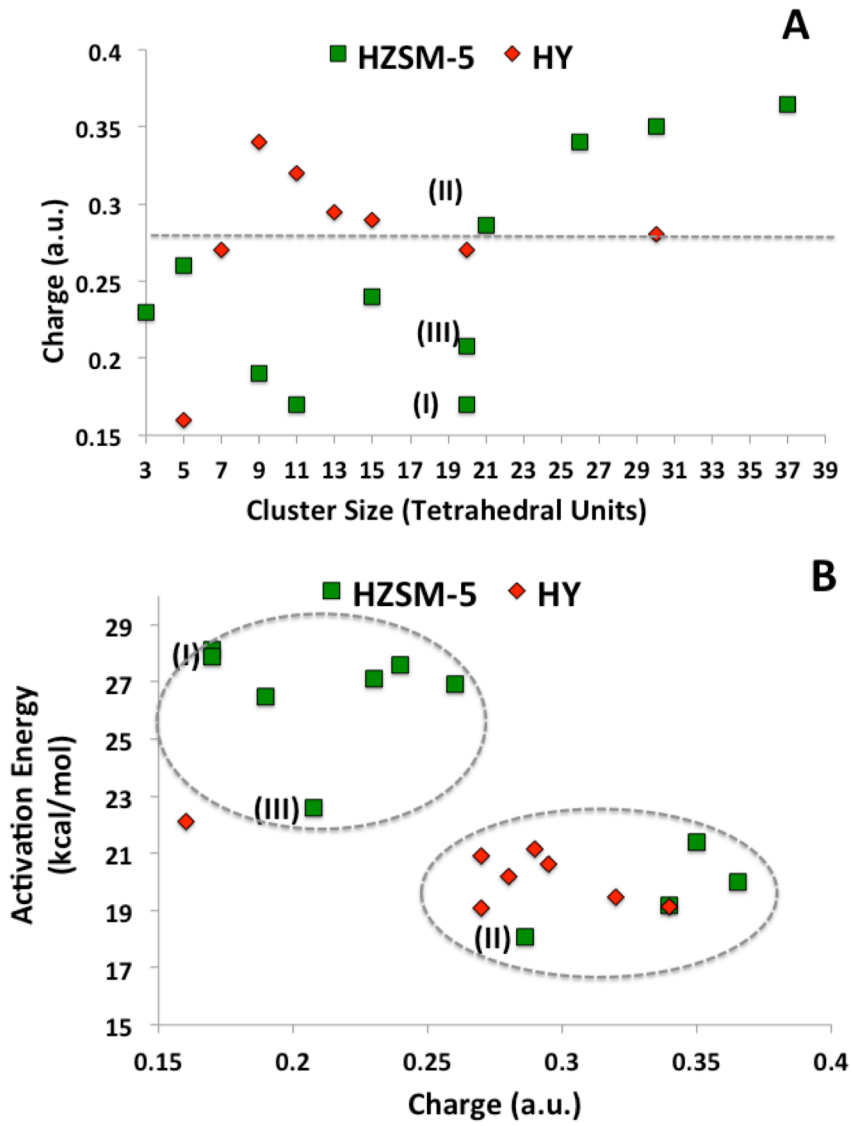

Figure 2.8: Dependence of active-site charge with respect to (A) system size and (B) bare electronic activation energy in both HZSM-5 and HY, where I, II, and III denote similarly-sized cluster models of HZSM-5 (defined previously in Sec. 2.1). The dashed line and circles appearing in (A) and (B) were added to serve as a visual aid.

These results suggest that sheer zeolite cluster size may be an insufficient criterion for converging barriers with respect to system size. The correlation between active-site charge in bare zeolite clusters, and resulting activation energy, suggests a new criterion for converging barriers with respect to zeolite cluster size. This approach is especially promising considering that determining active-site charges in bare zeolites does not require transition state searches, which can be computationally expensive.

2.3.4. Thermodynamic Energy Corrections

Dispersion corrections using the Grimme[37] approach, as implemented in the Jaguar[38] computational chemistry software suite, were applied to all structures (see Tables 2.1-2.8) these were not found to qualitatively influence the computed trends, likely because of the importance of site-specific hydrogen-bonding in zeolite-catalyzed aldol chemistry.

In the following tables, all energy correction terms were extracted from the normal mode analyses of the optimized reactant, transition, and product state at 298.15 K and 1atm. Final computed reaction and activation energies are reported within 0.1 kcal/mol, while individual corrections are reported to 0.01 kcal/mol accuracy to avoid round-off errors.

Outputs from Gaussian09[34] calculations include corrections to bring bare electronic energies to enthalpies and Gibbs free energies. Both of these corrections contain the zero-point vibrational energy correction, and the Gaussian Gibbs correction also contains the enthalpic correction. We wish to specify each of these corrections separately. To avoid double (and sometimes triple) counting each of these contributions,

we define the corrections in a way different from the Gaussian output. Our scheme below shows how we take Gaussian outputs to compute the individual corrections.

The full enthalpy of activation (ΔH_{act}) presented herein was obtained using the following calculation scheme:

$\Delta H_{act} = \Delta V_{act}^{0} + \Delta D3 + \Delta V_{ZPVE} + \Delta H_{corr}$, where (1)

$\Delta V_{act}^{0} = V_0^{\ddagger} - V_0^{R}$, (2)

$\Delta D3 = D3_0^{\ddagger} - D3_0^{R}$, (3)

$\Delta V_{ZPVE} = V_{ZPVE}^{\ddagger} - V_{ZPVE}^{R}$, and (4)

$\Delta H_{corr} = H^{\ddagger} - H^{R}$, where $H^{\ddagger} = H_{corr}^{\ddagger} - V_{ZPVE}^{\ddagger}$ and $H^{R} = H_{corr}^{R} - V_{ZPVE}^{R}$, (5)

where $V_0^{\ddagger}$ and V_0^{R} are the electronic ground state energies of the transition and reactant state, respectively, and $D_0^{\ddagger}$ and D_0^{R} are the respective Grimme[1] Dispersion corrections. Enthalpy corrections are shown as $H_{corr}^{\ddagger}$ and H_{corr}^{R} and zero point vibrational energy (ZPVE) corrections, $V_{ZPVE}^{\ddagger}$ and V_{ZPVE}^{R}.

The full Gibbs free energy of activation (ΔG_{act}) was obtained in a similar fashion as follows:

$\Delta G_{act} = \Delta V_{act}^{0} + \Delta D3 + \Delta V_{ZPVE} + \Delta H_{corr} + \Delta G_{corr}$, where

$\Delta G_{corr} = G^{\ddagger} - G^{R}$, where $G^{\ddagger} = G_{corr}^{\ddagger} - H_{corr}^{\ddagger}$ and $G^{R} = G_{corr}^{R} - H_{corr}^{R}$,

where ΔV_{act}^{0}, $\Delta D3$, ΔV_{ZPVE} , and ΔH_{corr} were defined previously in equations (2)-(5) and $G_{corr}^{\ddagger}$and G_{corr}^{R} are the free energy corrections, respectively.

The full enthalpy (ΔH_{RXN}) and Gibbs free energy (ΔG_{RXN}) of reaction were obtained in a similar manner using corrections corresponding to the product state, instead of the transition state (‡). Gas phase corrections were also computed according to this scheme, excluding dispersion corrections,

2.3.4.1 Energy corrections for all HZSM-5 clusters

Table 2.1: Activation energy corrections (kcal/mol) at 298.15 K for the keto/enol tautomerization of Acetone in HZSM-5.

Cluster Size	ΔV_{act}^{0}	$\Delta D3$	ΔV_{ZPVE}	ΔH_{corr}	ΔG_{corr}	ΔH_{act}	ΔG_{act}
3	27.1	-2.05	-2.45	-0.91	3.22	21.7	24.9
5	26.9	-2.71	-1.81	-1.12	4.01	21.2	25.2
9	26.5	-1.66	-1.80	-0.85	2.54	22.2	24.7
11	28.1	-3.14	-1.29	-1.00	3.57	22.7	26.3
15	27.6	-2.67	-1.35	-0.99	3.03	22.6	25.6
20 (I)	27.9	-0.32	-1.44	-0.92	2.56	25.2	27.8
21 (II)	18.1	-0.96	-0.31	-0.70	2.06	16.1	18.1
20 (III)	22.6	-2.22	-1.29	-0.85	2.59	18.3	20.8
26	19.2	-1.98	-1.79	-0.15	1.64	15.3	17.0
30	21.4	0.59	-1.06	-0.95	3.01	20.3	23.3
37	20.0	-0.93	-1.73	-0.64	1.13	16.7	17.9

Table 2.2: Reaction energy corrections (kcal/mol) for the keto/enol tautomerization of Acetone in HZSM-5.

Cluster Size	ΔV_{RXN}^{0}	$\Delta D3$	ΔV_{ZPVE}	ΔH_{corr}	ΔG_{corr}	ΔH_{RXN}	ΔG_{RXN}
3	23.3	-2.09	0.67	-0.52	2.24	21.4	23.6
5	25.0	-2.62	0.80	-0.70	2.88	22.5	25.4
9	21.0	-1.24	0.74	-0.49	1.63	20.0	21.6
11	24.7	-1.90	1.04	-0.47	2.00	23.4	25.4
15	25.6	-2.21	1.05	-1.11	2.55	23.3	25.9
20 (I)	25.0	0.23	0.97	-0.48	1.50	25.7	27.2
21 (II)	12.4	-0.72	2.10	-0.31	1.07	13.4	14.5
20 (III)	21.6	-2.05	0.97	-1.06	2.30	19.5	21.8
26	15.5	-1.59	0.82	0.26	0.97	15.0	16.0
30	17.4	0.48	1.21	-0.37	1.22	18.7	19.9
37	18.4	-0.98	0.71	-0.25	0.13	17.9	18.0

Table 2.3: Energy corrections (kcal/mol) for the condensation reaction between formaldehyde and acetone enol in an 11T cluster model of HZSM-5.

	ΔV^0	$\Delta D3$	ΔV_{ZPVE}	ΔH_{corr}	ΔG_{corr}	ΔH	ΔG
V_{act}	2.0	-1.41	-0.58	-1.18	3.30	-1.17	2.13
V_{rxn}	-26.1	-0.04	2.62	-0.97	2.35	-24.45	-22.11

2.3.4.2 Energy corrections for all HY clusters

Table 2.4: Activation energy corrections (kcal/mol) for the keto/enol tautomerization of Acetone in HY.

Cluster Size	ΔV^0_{act}	$\Delta D3$	ΔV_{ZPVE}	ΔH_{corr}	ΔG_{corr}	ΔH_{act}	ΔG_{act}
3	21.4	-1.65	-2.25	-0.94	3.38	16.6	20.0
5	22.1	-1.26	-2.27	-0.73	2.35	17.9	20.2
7	19.1	-0.69	-2.16	-0.73	1.88	15.6	17.4
9	19.1	-1.17	-1.97	-0.86	2.60	15.1	17.7
11	19.3	-1.04	-1.86	-1.00	2.56	15.4	18.0
13	19.1	-1.01	-2.00	-0.87	2.49	15.2	17.7
15	19.1	-0.99	-1.96	-0.87	2.61	15.3	18.0
20	20.9	-1.36	-1.94	-0.84	2.50	16.8	19.3
30	21.2	-1.34	-1.46	-0.84	2.60	17.6	20.2

Table 2.5: Reaction energy corrections (kcal/mol) for the keto/enol tautomerization of Acetone in HY.

Cluster Size	ΔV^0_{RXN}	$\Delta D3$	ΔV_{ZPVE}	ΔH_{corr}	ΔG_{corr}	ΔH_{RXN}	ΔG_{RXN}
3	17.9	-1.68	0.75	-0.51	2.20	16.5	18.7
5	18.5	-1.21	0.49	-0.31	1.21	17.5	18.7
7	15.6	-0.58	0.58	-0.28	0.63	15.4	16.0
9	16.2	-0.68	0.81	-0.43	1.24	16.0	17.2
11	16.4	-0.54	0.95	-1.17	2.03	15.6	17.7
13	16.2	-0.95	0.81	-0.50	1.58	15.6	17.2
15	16.5	-0.95	0.81	-0.49	1.64	15.9	17.5
20	19.1	-1.31	0.58	-0.41	1.19	18.0	19.2
30	20.3	-1.28	0.81	-0.47	1.66	19.4	21.0

Table 2.6: Energy corrections (kcal/mol) for the condensation reaction between formaldehyde and acetone enol in an 11T cluster model of HY.

	ΔV^0	$\Delta D3$	ΔV_{ZPVE}	ΔH_{corr}	ΔG_{corr}	ΔH	ΔG
V_{act}	0.37	-0.70	-1.00	-0.66	1.58	-2.00	-0.42
V_{rxn}	-25.4	1.17	2.73	-0.53	0.94	-22.05	-21.10

2.3.4.3 Energy corrections for gas-phase, uncatalyzed reaction

Table 2.7: Energy corrections (kcal/mol) for the gas-phase keto/enol tautomerization of acetone.

	ΔV^0	ΔV_{ZPVE}	ΔH_{corr}	ΔG_{corr}	ΔH	ΔG
V_{act}	68.2	-3.36	-0.38	1.27	64.4	65.7
V_{rxn}	12.7	0.76	-0.37	1.54	13.1	14.7

Table 2.8: Energy corrections (kcal/mol) for the gas-phase condensation reaction between formaldehyde and acetone enol.

	ΔV^0	ΔV_{ZPVE}	ΔH_{corr}	ΔG_{corr}	ΔH	ΔG
V_{act}	15.0	-0.71	-1.42	4.12	12.9	17.0
V_{rxn}	-22.0	2.92	-1.16	3.46	-20.2	-16.8

2.4 Summary and Concluding Remarks

We have applied DFT to model the mixed aldol condensation reaction between acetone and formaldehyde in HY and HZSM-5 acid zeolites. This reaction is an important prototypical carbon-carbon bond-forming reaction, requiring study to optimize biofuel and biomass-based chemical production processes. We have applied the B3LYP/6-311G(d,p) model chemistry and have computed all relevant energy corrections; i.e., Grimme dispersion, zero-point vibrational energy, enthalpy, and free energy corrections. We have studied this mixed aldol condensation in two steps: tautomerization and condensation, and have shown that both HY and HZSM-5 greatly reduce the activation energies of both steps relative to the gas-phase barriers, through extensive zeolite-guest hydrogen bonding. Using cluster models with 11 tetrahedral atoms ("11T" clusters) for both zeolites, we have found that acetone keto/enol tautomerization remains the rate-determining step of this mixed aldol condensation in zeolites, consistent with the mechanism in homogeneous acid catalysis.

We have examined the convergence of acetone tautomerization barriers with respect to cluster size for both HY and HZSM-5 zeolites. We considered cluster sizes 3T-30T for HY, and 3T-37T for HZSM-5. For HY, this barrier was found to converge relatively rapidly to ~20 kcal/mol for a cluster of size 11T, which does not complete the HY supercage. In contrast, the tautomerization barrier in HZSM-5 was found to reach an initial plateau value of ~28 kcal/mol for clusters in the broad range 3T-20T. For HZSM-5 clusters larger than 20T, well beyond the completion of an HZSM-5 10-ring, the acetone tautomerization barrier converges to ~20 kcal/mol. The smallest HZSM-5 cluster that produces the converged barrier includes 10-rings from both straight and sinusoidal

HZSM-5 channels. We speculate that the breadth and stability of the 3T-20T plateau for HZSM-5 may indicate chemical relevance for this higher activation energy, pertaining possibly to zeolite catalysis on Brønsted acid sites on external surfaces of HZSM-5. Further study is required to investigate this idea.

Our results show that completing a zeolite pore surrounding a Brønsted acid site may be insufficient to converge activation energies, especially for HZSM-5. We found instead a strong correlation between active-site charge – summing ESP charges over O2-Al-O1-H_z atoms in bare zeolites – and the corresponding acetone tautomerization barrier, especially for HZSM-5. The active-site charge convergence criterion is especially promising because determining active-site charges in bare zeolites does not require transition state searches. More research is required to determine why the dependence of active-site charge on cluster size is different for different zeolite frameworks.

CHAPTER 3
ON THE RATIONAL DESIGN OF ZEOLITE CLUSTERS

3.1 Introduction

In Chapter 2 we used cluster models of zeolites to model the mixed aldol condensation reaction between acetone and formaldehyde catalyzed by HZSM-5 or HY. Finite cluster models of zeolite crystals have been extensively employed to understand reactive and adsorptive processes in zeolites of various framework types.[29] Convergence with respect to zeolite cluster size is possible despite the presence of long-range interactions, because the slowly varying, long-range contributions to reaction and activation energies—energy differences between nearby configurations—essentially cancel for large enough but finite cluster sizes[30]. It is not obvious, however, how large zeolite clusters need to be for such cancellation to occur. In the present study, we perform systematic computational tests on zeolite cluster models in search of simple rules that govern system-size convergence of zeolite-guest interactions. Notably missing in the literature is a systematic method for constructing optimal zeolite clusters. The challenge thus remains to determine optimal cluster sizes, and perhaps more important, to determine optimal methods for building optimal clusters.

Here we address this issue by applying DFT to compute reaction energies for two processes relevant to the zeolite-catalyzed conversion of biomass: (1) the keto-enol tautomerization of acetone (Fig. 3.1A), which is the rate-limiting step in aldol condensation, [29] and (2) the protonation and ring opening of furan (Figs. 3.1B and 3.1C, respectively), which are initial steps in biofuel production via the catalytic fast pyrolysis of cellulose.[49-50]

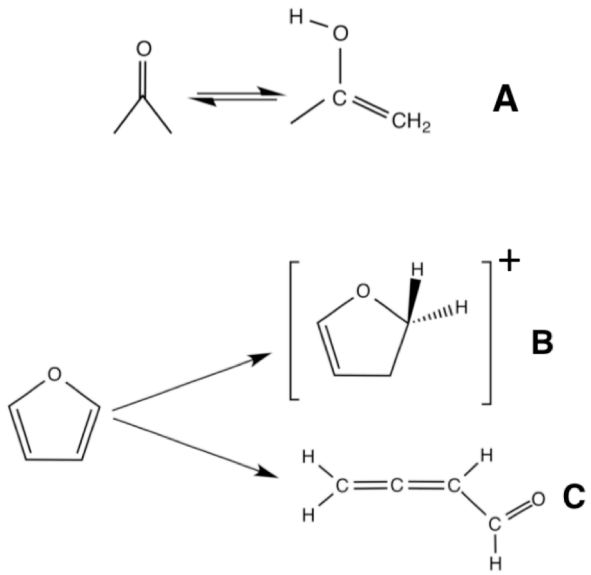

Figure 3.1: Reactions for (A) keto/enol tautomerization of acetone, (B) protonation of furan, an (C) ring opening of furan.

3.2 Methods

3.2.1 Reaction Processes

To elucidate the general principles that may guide cluster construction, we investigate four reactant-product pairs. The first two systems arise from the rate-determining step in the zeolite catalyzed aldol condensation between acetone and formaldehyde (Fig. 3.1A).[29] These are

1. Acetone (reactant) and enol (product) adsorbed in HZSM-5.
2. Acetone (reactant) and enol (product) adsorbed in HY.

In the final two systems, the reactant is furan adsorbed in HZSM-5. The products are:

3. Positively-charged derivative of furan, protonated at the C2 position (shown in Fig. 3.1B).
4. Neutral ring-opened species (shown in Fig. 3.11C).

Both of these furan derivatives are key intermediates in the HZSM-5 catalyzed conversion of furan to benzofuran, [27] which leads to biofuel production via the catalytic fast pyrolysis of cellulose. We focus herein on computing reaction energies instead of activation energies for the following two reasons: first, for computational ease as we consider below systems with as many as 166 T-atoms; second, the insights from the present study extend to the convergence rates of activation energies as well. To see why, we note that when computing energy differences between nearby guest configurations, the convergence rate of the long-range component (arising from electrostatics) depends on how much the charge distributions differ – the greater the difference, the bigger the cluster required to converge the energy difference. Perhaps the most demanding case involves a neutral reactant that becomes a charged product (or vice versa). We have

considered precisely this situation as shown in Fig. 3.1B, and as such our study elucidates the relevant aspects of zeolite cluster convergence for catalytic studies.

To investigate the issue of charge distributions, we consider a variety of reactions in Fig. 3.1 including neutral → neutral and neutral → charged processes, to test whether the presence of charge influences convergence properties of zeolite clusters. We develop two distinct and simple approaches for rational construction of zeolite clusters. One approach pays homage to the anisotropic nature of zeolite structures, by counting framework bonds from a Brønsted acid-site aluminum atom. The other approach is based on including zeolite atoms that fall within multi-centered spherical cutoffs, and hence is more isotropic in nature. We demonstrate below that the approach using multi-centered spherical cutoffs exhibits both smoother convergence, and convergence at smaller system sizes. In addition, we find that a 5-Å cutoff is sufficient to converge a variety of reaction energies as long as the cutoff is measured from all relevant reactant, product, and active-site atoms.

3.2.2 Zeolite Models

Guest molecule coordinates are taken from previously optimized clusters in our earlier studies.[27, 29] Zeolite clusters are carved out from the periodic crystal, terminated at either Si or O, and capped with hydrogen atoms.[31,32] The Si-H bond lengths were set to 1.4 Å, while O-H bond lengths were set to 0.9 Å. As in our previous work (see Chapter 2) [27, 29], the Brønsted acid site in HZSM-5 was chosen to be O(13), located at the intersection of the straight and zig-zag channels. The HY cluster models were centered on O(1) in the 12-ring window with the Brønsted acid site pointed directly into the

supercage. The applicability of the O(1) site as the Brønsted acid site was previously determined to be a catalytically relevant position.[30]

We have systematically expanded the zeolite clusters in the following two ways: (*i*) by counting framework bonds (so-called "*n*-bond" clusters) and (ii) by applying multi-centered spherical cutoffs (so-called "delta" or "d" clusters), as described below.

3.2.2.1 N-bond Clusters

N-bond clusters were constructed by including all framework atoms that are within *n* bonds from the Brønsted acid-site aluminum atom, where *n* ranges from 1 to 11 (illustrated in Figure 3.2 for *n* = 3 and 5). This method requires no *a priori* knowledge of guest molecule coordinates, and guarantees the construction of well-connected zeolite clusters with no dangling atoms.

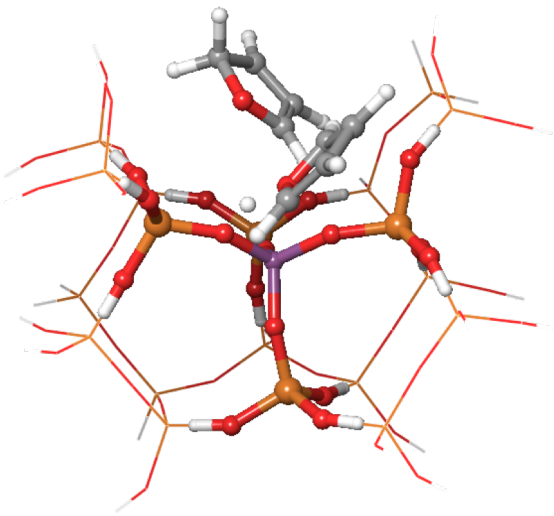

Figure 3.2: Illustration of an *n*-bond cluster of HZSM-5, where furan and protonated furan are shown as guest molecules. The tubes correspond to n= 3 and n = 5 is shown as wire mesh (shown from the perspective looking down the intersection of the 10T straight and 10T zig-zag channels).

3.2.2.2 Delta Clusters

Alternatively, a zeolite cluster can be defined on the basis of proximity to the reacting atoms, e.g., relevant guest configurations and the Brønsted acid site. However, care must be taken to produce well-connected clusters, as described below. In particular, the delta approach is based on the following two-step procedure: (*i*) include all zeolite atoms that fall within the union of several spheres – all with the same radius δ – but centered at the following various points: Brønsted acid site oxygen atoms, and each reactant and product guest atom (see Fig. 3.3A). This approach requires initial guesses for adsorbed reactant and product geometries, which may be obtained relatively cheaply with low level pre-optimizations. (*ii*) If a framework atom A does not fall within the spherical cutoffs in step (*i*), but is bonded to two atoms that are included in step (*i*), atom A is included in the delta cluster. The delta method ensures that the cluster includes framework atoms that interact most strongly with the guest molecules. The final cluster used in computations is defined as the union set of all framework atoms selected in steps (*i*) and (*ii*) above (see Fig. 3.3B). This procedure has been implemented systematically with an automated script using the Schrödinger Python API, and is available from Schrödinger.

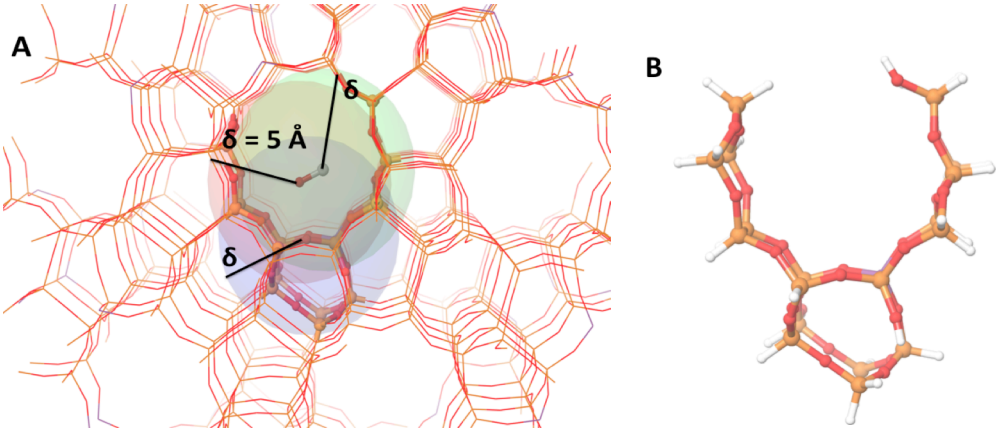

Figure 3.3: (A) Illustrated scheme for constructing delta cluster of HZSM-5 where carbon monoxide (CO) is used as an example guest molecule. The three spheres centered on guest C, guest O, and zeolite acid site O (all with the same radius, d = 5 Å), are represented by different colors. The union set of the three spheres, plus four required connecting atoms (see text), yields the resultant delta cluster shown in (B), where CO has been removed for clarity, and dangling bonds have been capped with hydrogens.

3.2.3 Computational Details

We seek to understand the convergence of long-range interactions in zeolitic host-guest systems with respect to zeolite cluster size. To this end, we calculate single-point energy differences between the product and reactant states as a function of *n* and δ in *n*-bond and delta clusters, respectively. The single-point calculations ensure that atomic positions remain constant across clusters, hence providing rigorously comparable systems. Therefore, the cluster size dependence of the energy differences can be solely attributed to the convergence of long-range interactions. This procedure has the added advantage of being fast enough that a large number of clusters can be evaluated to discern convergence trends. For example, a single-point calculation on the 78T HZSM-5 *n*-bond cluster required ~6 hours while an optimization on the same system required ~160 hours. We also geometry-optimize selected clusters to confirm the relevance of the single-point energy differences based on our previously published work on these reaction systems. In these optimizations, terminal –H and –OH groups were frozen in their crystallographic positions; all other atoms were free to move.

The B3LYP[35] hybrid density functional was used with the 6-311G(d,p) [36]basis set as implemented with the electronic structure program Jaguar[38]. This model chemistry has been previously shown by Fermann *et al*. to capture ~90% of activation energies for proton transfer processes in zeolites[30]. Moreover, accurate barriers for the acid-catalyzed aldol chemistry were recently using this model chemistry.[29] We have determined the Gibbs energies of reaction in select delta clusters within the harmonic oscillator approximation, and have also implemented dispersion corrections using the Grimme[24] approach (see Section 3.3.5); these were not found to influence the reported trends.

3.3 Results and Discussion

Here we report the outcome of two different approaches for the rational construction of cluster models of zeolite crystals. First, we analyze and compare the differences between the two approaches for different reaction systems; (1) the keto/enol tautomerization of acetone in HZMS-5 and HY zeolites; (2) the protonation of furan; and (3) the ring opening of furan in HZSM-5. Then, we describe a general protocol for systematically constructing cluster models of zeolite crystals.

3.3.1 Acetone Tautomerization in Clusters of HZSM-5 and HY

The tautomerization of acetone in both HZSM-5 and HY follows a concerted mechanism and begins with the adsorption of acetone to the zeolite Brønsted acid site.[29] Once acetone is adsorbed, the zeolite acid site protonates the carbonyl oxygen while the adjoining methyl carbon is deprotonated, thereby regenerating the zeolite catalyst.[29] Figure 3.4 shows single-point energy differences and optimized reaction energies for this reaction in both zeolites. Figures 3.4A and 3.4B demonstrate convergence for the HY *n*-bond and delta clusters, respectively. Figures 3.4C and 3.4D show the corresponding data for HZSM-5 *n*-bond and delta clusters, respectively.

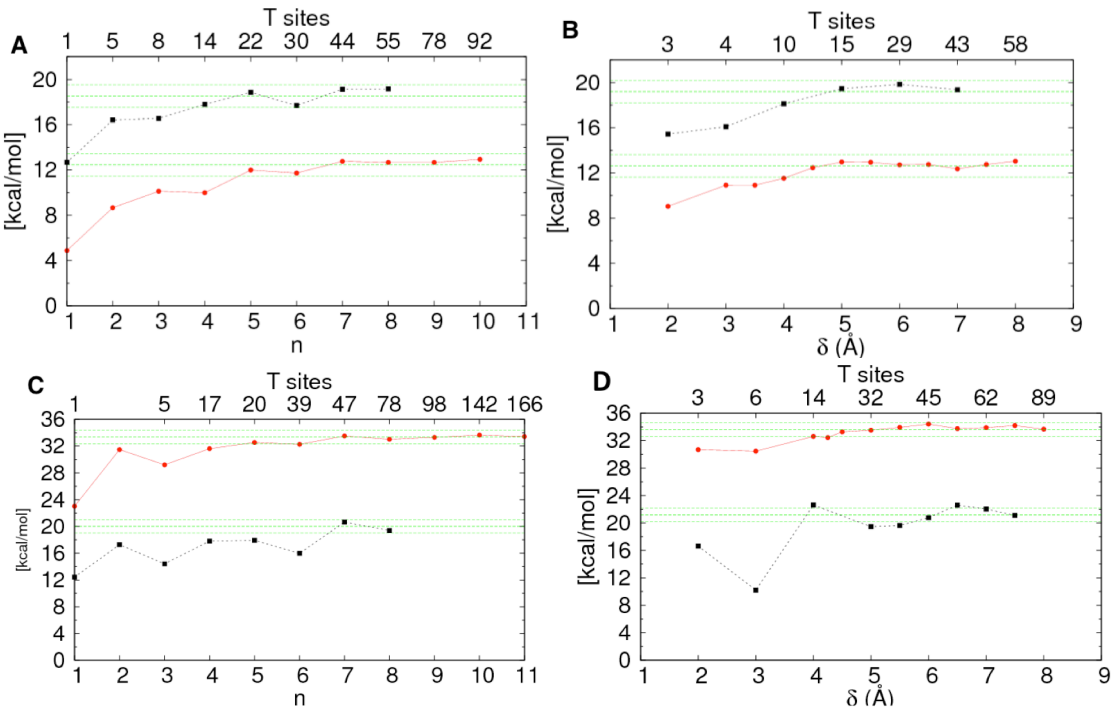

Figure 3.4: The dependence of reaction energies for the tautomerization of acetone in various size clusters of HY (A & B) and HZSM-5 (C & D); n-bond clusters (A & C) and delta clusters (B & D). All values shown in black correspond to optimized reaction energies and those in red to single point energy differences. The dashed green lines represent the zone of convergence to chemical accuracy (± 1 kcal/mol).

In both zeolites, the converged single-point reaction energies using n-bond clusters agree well with the corresponding energies obtained using delta clusters. In Figure 3.4A, single point energies in *n*-bond clusters of HY converge to 12.0 kcal/mol when $n \geq 5$. The HY delta clusters mirror the same trend for the single-point energy differences (Fig. 3.4B). When $\delta \geq 4$ Å, single-point energy differences converge to ~12.2 kcal/mol (Fig. 3.4B). In the case of HZSM-5 the single-point energies of the *n*-bond clusters converge to ~33.0 kcal/mol for values of $n \geq 5$ (Fig. 3.4C). This convergence trend is mirrored by the single-point energy differences in the delta clusters (Fig. 3.4D). When $\delta \geq 4$ Å, energy differences converge to ~33.5 kcal/mol in HZSM-5 (Fig. 3.4D). Although the single-point energy differences converge to the same value with both approaches, it is important not to over-interpret the results of single-point energy calculations. Since single points do not provide optimized geometries they are utilized only as a tool to gauge convergence of long-range interactions.

Optimized reaction energies of selected *n*-bond and delta clusters of HY and HZSM-5 reveal similar convergence trends with respect to system size (see Fig. 3.4A, B & 3.4C, D)). In *n*-bond clusters of HY and HZSM-5, reaction energies converge to 18.8 kcal/mol and 20.5 kcal/mol, respectively (Fig. 3.4A & 3.4C). In delta-clusters of HY and HZSM-5, energies converge to ~19.5 kcal/mol and 21.0 kcal/mol, respectively (Fig. 3.4D and 3.4B, respectively). Both of our approaches to cluster construction yield optimized reaction energies in the two zeolites that agree well with the previously determined reaction energies at the same model chemistry. [5, 29] Migues *et al*. reported 20.3 and 18.4 kcal/mol for a 30T cluster of HY, and a 37T cluster of HZSM-5,

respectively.[29] Boekfa *et al*. reported essentially identical results in a 34T cluster of HZSM-5.[5]

Although the two approaches converge to accurate reaction energies for both zeolites, they do not converge at the same system size. In fact, the optimizations reveal that the *n*-bond clusters of HZSM-5 do not converge until $n \geq 7$ (Fig. 3.4C); a 47T cluster. In comparison, the delta clusters of HZSM-5 converge when $\delta \geq 4.0$ Å (Fig. 3.4D); this system size corresponds to 14T. Similarly in HY, delta clusters converge at smaller system sizes compared to *n*-bond clusters. In Figure 3.4B, optimized reaction energies in HY converge when $\delta \geq 4.0$ Å (10T) compared to *n*-bond clusters where convergence is not reached until $n \geq 4.0$ Å (14T). Our results demonstrate that clusters constructed using the multi-centered spherical cutoffs converge reaction energies for the tautomerization of acetone in HZSM-5 and HY at smaller system sizes than the corresponding n-bond clusters.

3.3.2 Protonation of Furan in Cluster Models of HZSM-5

In this reaction, the Brønsted acid site in HZSM-5 donates a proton to an adsorbed furan at its C2 position, forming a positively charged intermediate[27]. Figure 3.5 shows single-point energy differences and optimized reaction energies for the protonation reaction of furan in *n*-bond (Fig. 3.5A) and delta clusters (Fig. 3.5B) of HZSM-5. Both methods of cluster construction agree reasonably well with each other.

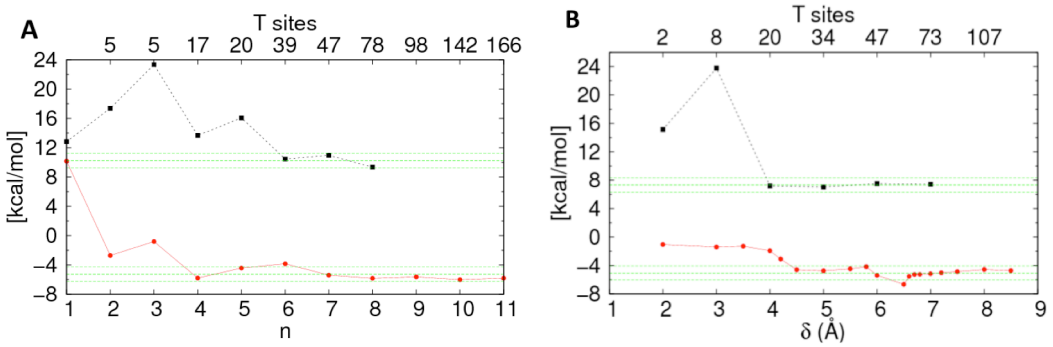

Figure 3.5: The dependence of reaction energies for the protonation of furan in various size clusters of HZSM-5; *n*-bond clusters (A) and delta clusters (B). In both 5A & 5B, values shown in black correspond to optimized reaction energies and those in red to single-point energy differences. The dashed green lines represent the zone of convergence to chemical accuracy (± 1 kcal/mol).

In Figure 3.5A, single-point energies converge to ~ –5.4 kcal/mol at values of $n \geq 7$ in HZSM-5. Optimizations reveal similar convergence trends at $n \geq 7$ with reaction energies of ~10.0 kcal/mol (Fig. 3.5A). Recall that n = 7 corresponds to a total system size of 47 tetrahedral units of HZSM-5. In Figure 3.5B, single point energies converge to ~ –5.0 kcal/mol at $\delta \geq 4.5$ Å, and optimized energies converge to ~7.2 kcal/mol at smaller values of δ (δ=4.0 Å). In this reaction system, a value of δ = 4 Å corresponds to a system size of 20T.

Both of the approaches to cluster construction, *n*-bond and delta, yield reaction energies for the protonation reaction of furan that compare reasonably well to the previously reported value of 12.7 kcal/mol in HZSM-5.[27] In this previous study, an embedded (ONIOM) approach was followed using a 132T QM/MM cluster of HZSM-5, in which an 11T layer was treated quantum mechanically. Our results for the protonation of furan in HZSM-5 also demonstrate that delta clusters converge reaction energies at smaller system sizes compared to *n*-bond cluster models.

3.3.3 Ring Opening of Furan in Cluster Models of HZSM-5

Furan adsorbed in HZSM-5 can also be transiently protonated at the O1 site, leading to a neutral ring-opened product.[27] Figure 3.6 shows single-point and optimized reaction energies for the ring opening of furan in n-bond (Fig. 3.6A) and delta clusters (Fig. 3.6B) of HZSM-5.

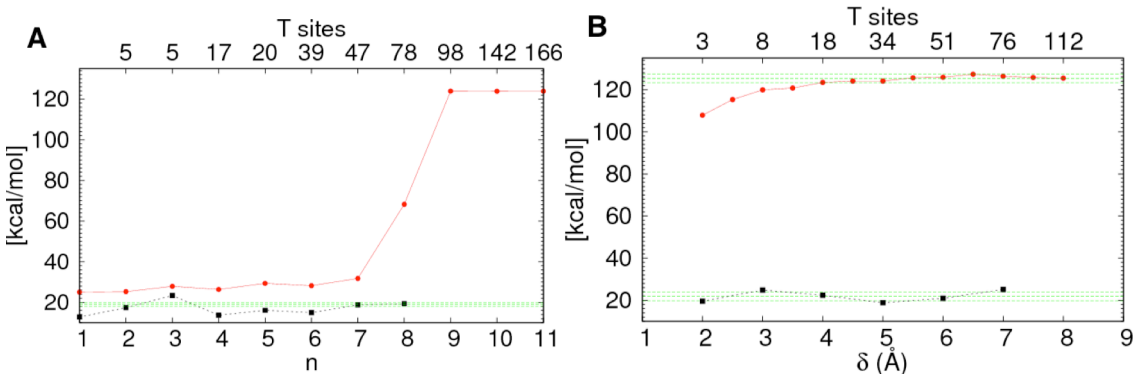

Figure 3.6: The dependence of reaction energies for the ring opening of furan in various size clusters of HZSM-5; *n*-bond clusters (A) and delta clusters (B). In both 6A and 6B, values shown in black correspond to optimized reaction energies and those in red to single point energy differences. The dashed green lines represent the zone of convergence to chemical accuracy (± 1 kcal/mol).

Single point energies for the ring-opening reaction appear to converge to ~26 kcal/mol when n ≤ 7 (Fig. 3.6A). However at n = 8 a significant increase by ≥ 40 kcal/mol is observed and persists until energies converge to ~123.0 kcal/mol for values of $n \geq 9$. Upon optimization of the n-bond systems, this trend was not observed and energies quickly converged to ~ 18.6 kcal/mol when $n \geq 7$ (Fig. 3.6A). This behavior arises from the fact that the single-point studies on the ring-opened structure lock the product into a configuration that experiences severe steric repulsion with the opposite side of the HZSM-5 channel. As such, once the value of n increases to complete the channel, the reaction energy jumps precipitously. This may be viewed as an inherent limitation of studying single-points; instead, we view this as a limitation of the n-bond cluster construction method, as described below.

A similar trend in single point energies was not observed in cluster models constructed using multi-centered spherical cutoffs (Fig 3.6B). Even at the smallest values of delta, single point energy differences are >105 kcal/mol. When $\delta \geq 4.0$ Å, single point energies converge to ~123.4 kcal/mol and upon optimization energies converge to 18.5 kcal/mol at $\delta \geq 5.0$ Å (Fig 3.6B). A value of $\delta = 5.0$ Å corresponds to a system size of 34T in HZSM-5, significantly smaller than the n-bond system sizes necessary to converge energies. These delta-cluster results show that the multi-centered spherical cutoffs method correctly constructed clusters that reveal the strong steric hindrance even for the smallest values of δ.

Our reaction energy for the ring opening of furan is significantly higher (by ~7.5 kcal/mol) than the previously reported value of 11.0 kcal/mol.[27] However the previous study used an embedded QM/MM approach to model HZSM-5. Although the total

system size was 132T, only an 11T subunit surrounding the active site was modeled at the B3LYP/6-311G(d,p) model chemistry and the Universal Force Field (UFF) was used for the remaining MM layer.[27] Based on the excellent agreement between our computed reaction energies and those previously reported for the keto/enol tautomerization in HZSM-5 and HY at the same model chemistry,[29] we suggest that methodological differences may account for the discrepancy between reaction energies computed via quantum cluster and QM/MM techniques.

3.3.4 Generalized Protocol for Constructing Cluster Models of Zeolite Crystals

Here we describe a general procedure (Figure 3.7) for building zeolite clusters using the delta-cluster approach. Once one has identified a (*i*) reaction of interest, (*ii*) the zeolite type, and (*iii*) the acid site location, X-ray coordinates for the zeolite can be downloaded. The zeolite coordinates along with initial guesses for the reactant and product adsorbed guest geometries can be fed into the automated cluster-building script which uses the Schrödinger Python API. Initially a multi-centered spherical cutoff of δ = 7 Å should be applied to generate a large cluster, sufficient to further refine the guest molecule geometries (Fig. 3.7A). This choice of a 7 Å cluster represents a balance between the need to start with a large initial cluster to capture as many effects as possible, and the computational cost of pre-optimization on such a large cluster. After the δ = 7 Å "master" cluster is built, we suggest application of a low-level model (e.g., a generic force field such as UFF) to optimize the guest reactant and product geometries in a reasonable amount of time (Fig. 3.7B). Once the low-level optimization is complete, the

Python script is re-applied with a multi-centered spherical cutoff of $\delta = 5.0$ Å to generate a smaller, converged production cluster (Fig. 3.7C) for use in higher-level optimizations.

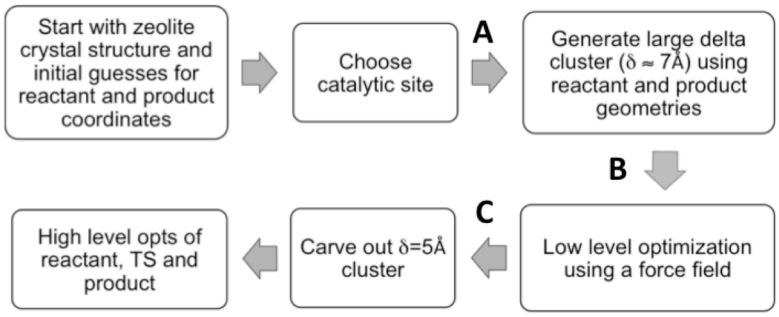

Figure 3.7: Flowchart illustrating a general procedure for constructing delta clusters of zeolites.

3.3.5 Thermodynamic Energy Corrections

We have determined the Gibbs energies of reaction in select delta clusters within the harmonic oscillator approximation (Figs. 3.8 &3.9), and have also implemented dispersion corrections using the Grimme[24] approach (Figs. 3.9-3.14). These were not found to influence the reported trends.

3.3.5.1 Gibbs Corrected Reaction Energies

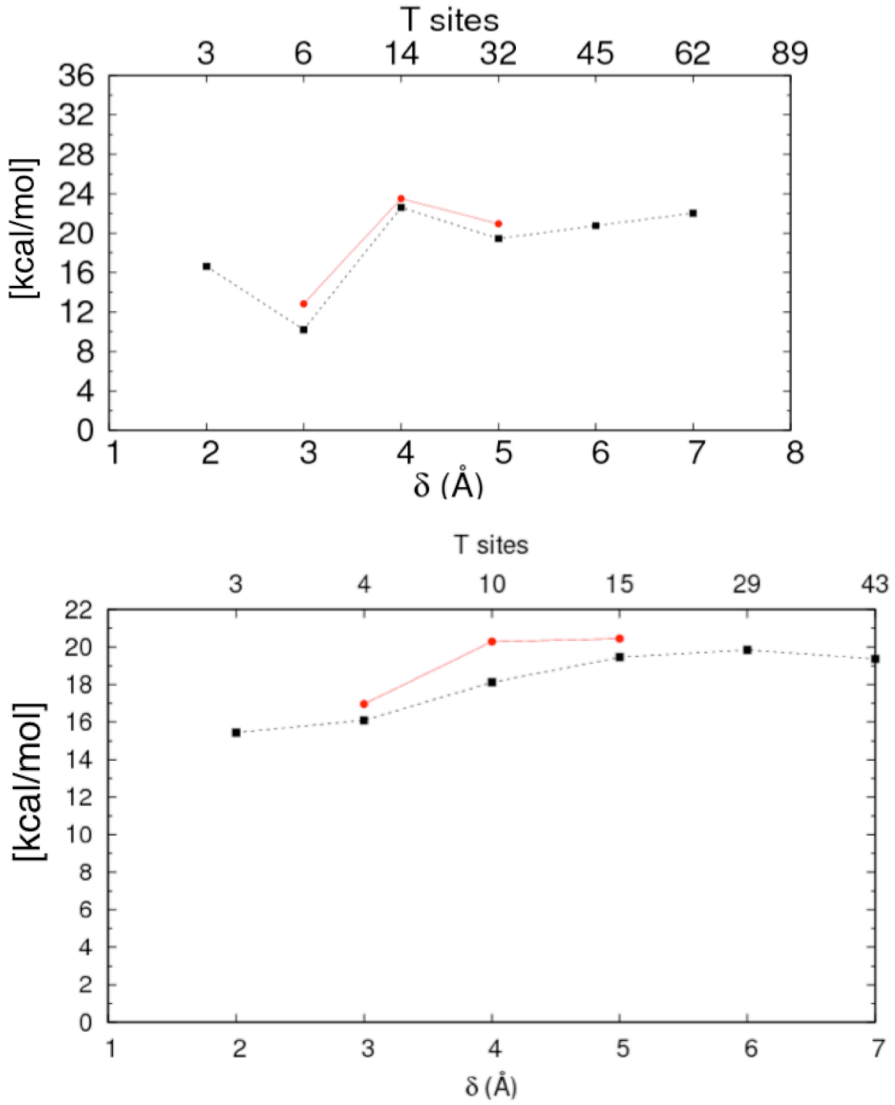

Figure 3.8: Reaction energies for the tautomerization of acetone in various size delta clusters of HZSM-5 (shown top). Reaction energies for the tautomerization of acetone in various size delta clusters of HY (shown bottom). Values shown in black correspond to the B3LYP/6-311G (d,p) optimized reaction energies and those in red correspond to B3LYP/6-311G (d,p) Gibbs reaction energies.

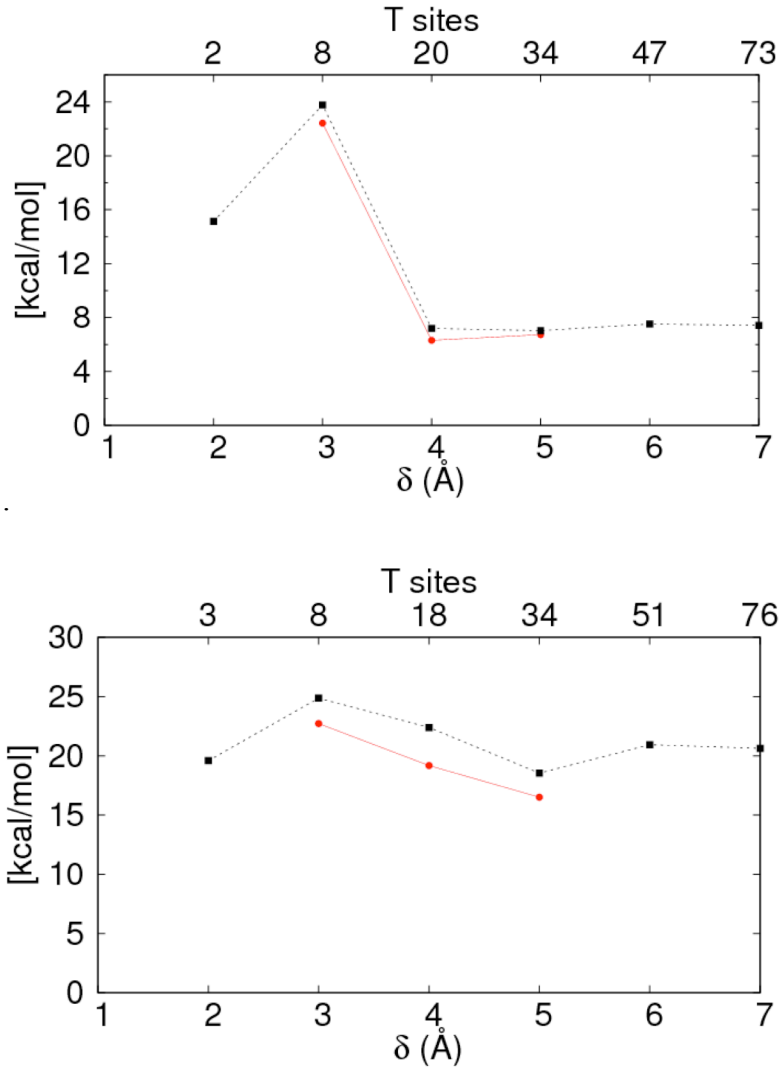

Figure 3.9: Reaction energies for the protonation of furan in various size delta clusters of HZSM-5 (shown top). Reaction energies for the ring-opening of furan in various size delta clusters of HZSM-5 (shown bottom). Values shown in black correspond to the B3LYP/6-311G (d,p) optimized reaction energies and those in red correspond to B3LYP/6-311G (d,p) Gibbs reaction energies.

3.3.5.2 Dispersion Corrected Reaction Energies

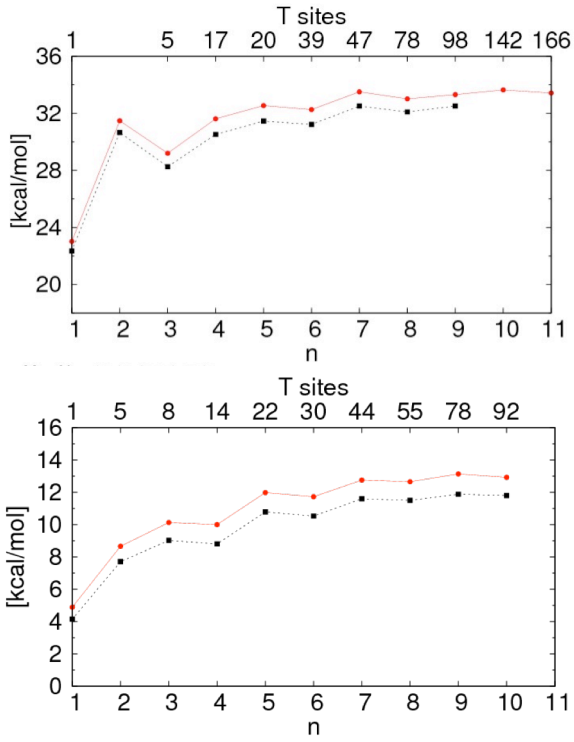

Figure 3.10: Single point reaction energy differences for the tautomerization of acetone in various size n-bond clusters of HZSM-5 (shown top). Single point reaction energy differences for the tautomerization of acetone in various size n-bond clusters of HY (shown bottom). Values shown in red correspond to B3LYP/6-311G (d,p) single point energies and those in black to D3 corrected single point energies.

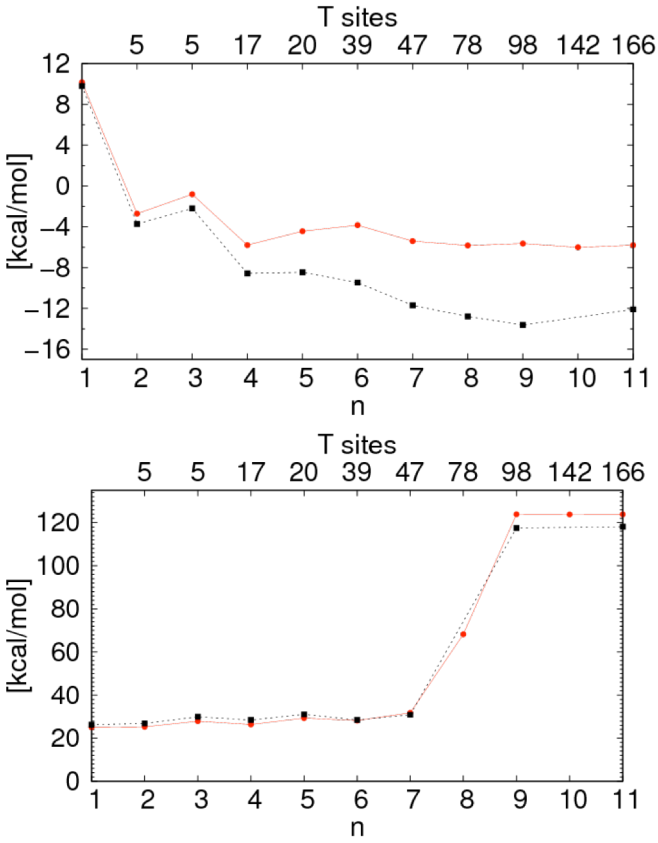

Figure 3.11: Single point reaction energy differences for the protonation of furan in various size n-bond clusters of HZSM-5 (shown top). Single point reaction energy differences for the ring-opening of furan in various size n-bond clusters of HZSM-5 (shown bottom). Values shown in red correspond to B3LYP/6-311G (d,p) single point energies and those in black correspond to D3 corrected single point energies.

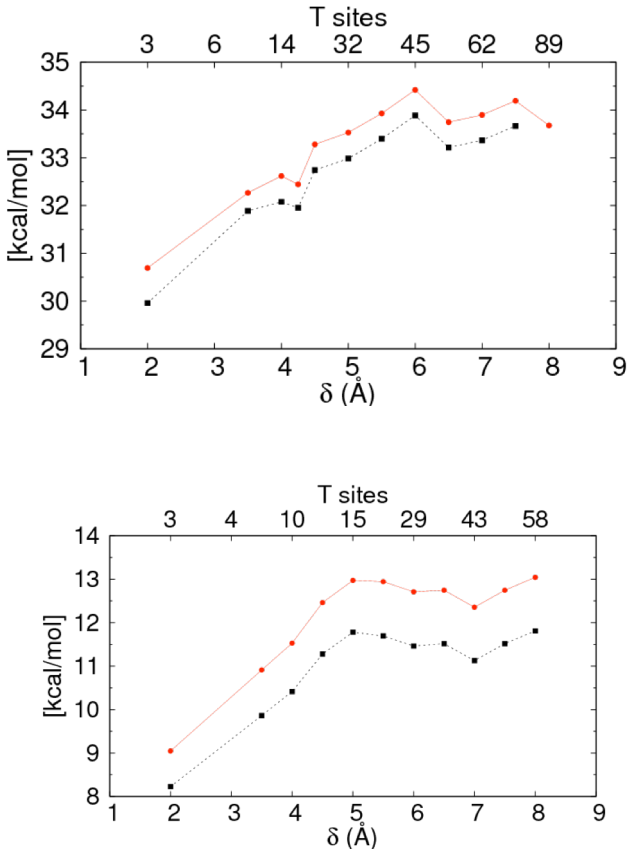

Figure 3.12: Single point reaction energy differences for the tautomerization of acetone in various size delta clusters of HZSM-5 (shown top). Single point reaction energy differences for the tautomerization of acetone in various size delta clusters of HY (shown bottom). Values shown in red correspond to B3LYP/6-311G (d,p) single point energies and those in black correspond to D3 corrected single point energies.

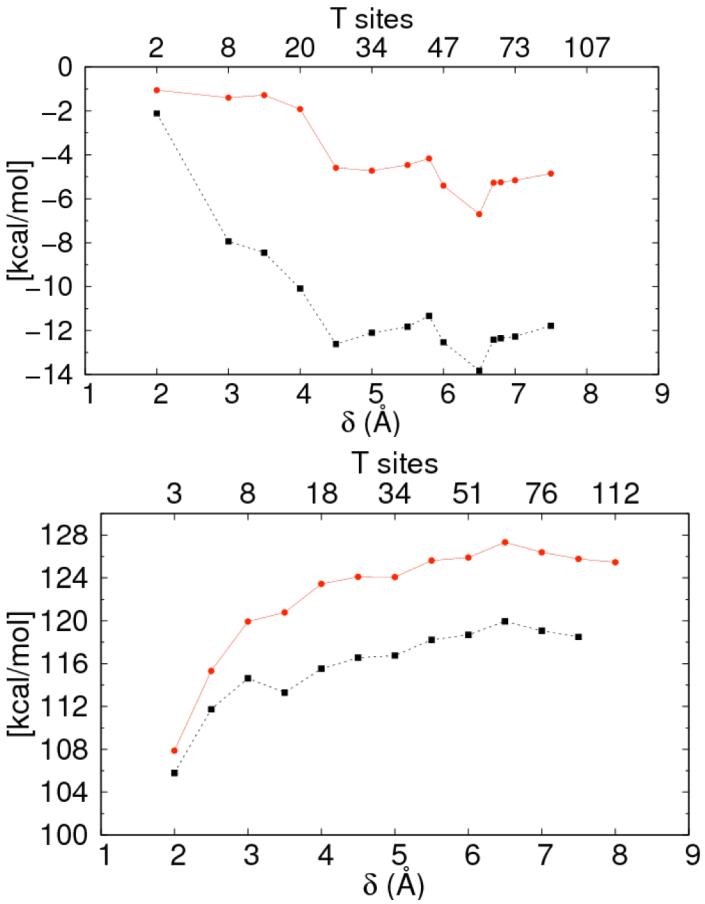

Figure 3.13: Single point reaction energy differences for the protonation of furan in various size delta clusters of HZSM-5 (shown top). Single point reaction energy differences for the ring-opening of furan in various size delta clusters of HZSM-5 (shown bottom). Values shown in red correspond to B3LYP/6-311G (d,p) single point energies and those in black correspond to D3 corrected single point energies.

3.4 Summary and Concluding Remarks

We have studied the convergence of zeolite cluster models due to the importance of simulating zeolite-catalyzed reactions, the presence of long-range interactions in zeolite-guest systems, and the general utility of finite cluster models. We have studied four reactions as platforms for understanding how convergence of reaction energies may vary for neutral → neutral and neutral → charged processes. In particular, we have applied DFT calculations to compute reaction energies for acid-zeolite-catalyzed processes related to the conversion of biomass: (1) the keto-enol tautomerization of acetone in HZSM-5 and HY and (2) the protonation and ring opening of furan in HZSM-5. To investigate cluster convergence, we have compared two rather distinct methods for building successively larger clusters: one method (denoted "*n*-bond") is based on counting bonds from a catalytic site, while the other method (denoted "delta") applies multi-centered spherical cutoffs from each guest reactant and product atom, and from the acid site.

We have investigated the convergence of reaction energies using both single-point calculations on clusters containing as many as 166 tetrahedral (T) atoms, and optimizations on clusters with as many as 78 T-atoms. For all the reactions we studied, the clusters generated with multi-centered spherical cutoffs yield converged reaction energies with smaller system sizes than by counting framework bonds. This method employing a single length scale (5 Å) converges reaction energies to within chemical accuracy (±1 kcal/mol), and includes between 15 and 34 T-atoms in the cluster depending on the process under study. Based on the general success of the delta-cluster method, we

suggest a general protocol for generating such clusters for subsequent use in computational zeolite science.

CHAPTER 4

Density Functional Theory Study of Mixed Aldol Condensation Reactions Catalyzed by HZSM-5

4.1 Introduction

In Chapter 3, we developed the delta cluster approach to constructing finite cluster models of zeolite crystals, in which contributions from slow-varying long range forces were convergent with respect to system size.[51] The delta approach to constructing finite clusters provides a well-defined prescription and employs a single length scale (δ = 5 Å) to converge reaction energies to within chemical accuracy (±1 kcal/mol)[51]. In Chapter 2, we focused on converging reaction energies in delta clusters and did not address convergence with respect to activation barriers. Although delta cluster give convergent reaction energies at δ = 5 Å for reaction systems involving both charged and neutral species, it is not clear that such convergence trends with respect to delta will persist in the case of activation barriers.

Here we have applied the delta cluster approach to model the mixed aldol condensation catalyzed by HZSM-5. We have examined two reaction systems relevant to biomass from our previous work[29] (see Chapter 2) to understand the convergence of activation barriers using delta clusters of HZSM-5. First, we have examined the unimolecular tautomerization reaction of acetone (see Fig. 4.1), the rate-determining step in condensation, and second the bimolecular condensation between the enol and formaldehyde (see Fig. 4.1I), in which a new carbon bond is built. We find that in both reaction systems, a $\delta \geq 4$ Å cutoff is sufficient to converge barriers.

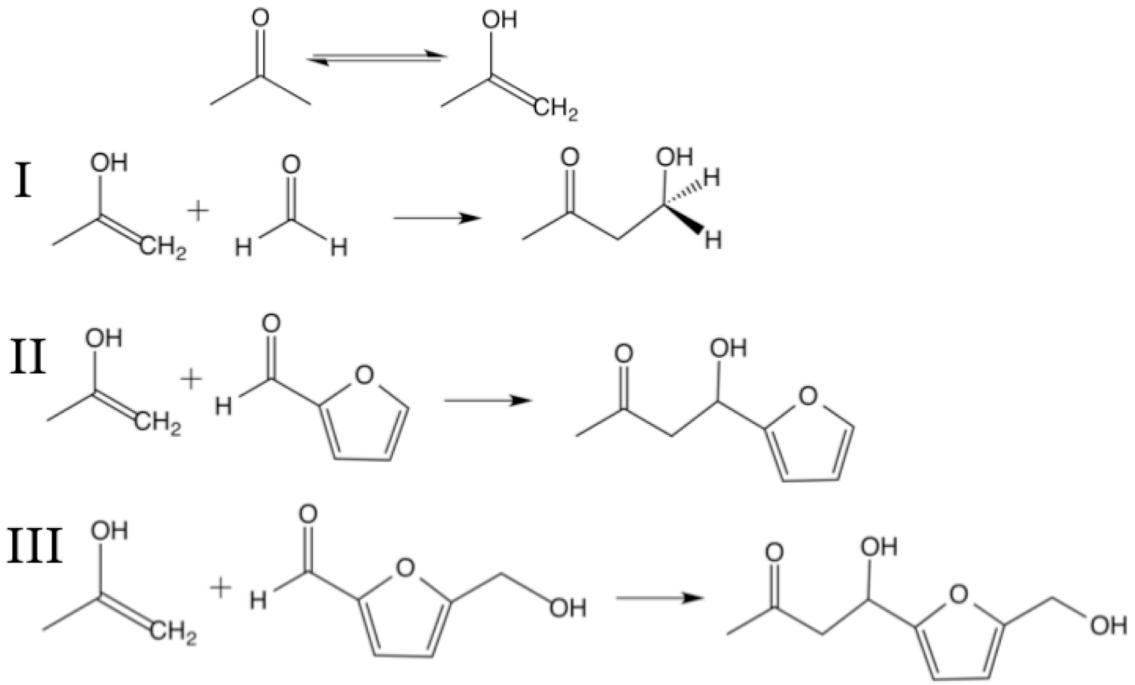

Figure 4.1: Reaction schemes for the keto-enol tautomerization of acetone (shown top) and the aldol condensation reaction between the acetone enol and (I) formaldehyde (II) furfural and (III) HMF.

We then proceed to investigate the relationship between activation energies and aldehyde size to understand the effect that increasing aldehyde size has on aldol condensation barriers. Moreover we seek to understand the effect confinement in the zeolite nanopore has on reaction mechanisms, compared to the homogeneous acid catalyzed mechanism (see Fig. 1.2). In this vein, we have examined two aldehydes as reactants in the aldol condensation with acetone, furfural (see Fig. 4.1II) and hydroxymethylfurfural (HMF) (see Fig. 4.1III). Furfural and HMF are biomass-derived feedstock chemicals, important in the production of octane grade fuels, and as precursors to plastics and other commodity organics[52]. Here we report activation barriers for the aldol condensation reaction between acetone and furfural and HMF in $\delta = 4$ Å (~34T) cluster models of HZSM-5.

4.2 Methods

4.2.1 Reaction Processes

In order to establish convergence of activation barriers in delta cluster models of HZMS-5, we investigate the mixed aldol condensation reaction between acetone and formaldehyde in two steps: (i) keto-enol tautomerization of acetone (Fig. 4.1) and (ii) condensation between the acetone enol and formaldehyde (Fig. 4.1 I). We then proceed to model condensation between the enol and more biomass-relevant aldehydes, such as furfural and HMF in delta clusters of HZSM-5 (Fig. 4.1 II & III).

4.2.2 Zeolite Models

In this study, we used delta clusters of zeolite crystals to model the acid catalyzed tautomerization of acetone (see Fig. 4.1) and subsequent aldol condensation with

formaldehyde, furfural and HMF (see Fig. 4.1 I, II & III). All clusters of HZSM-5 were constructed following the delta approach[51], outlined in Chapter 3. In short, this approach uses multi-centered spherical cutoffs – each centered about the guest molecule atoms and the zeolite Brønsted acid site oxygens – to incorporate all relevant zeolite framework atoms. For a more detailed description of the delta approach, the reader is referred to ref. 51. Since this method requires a priori knowledge of the guest molecule coordinates and Brønsted acid site, the delta clusters generated are reaction specific. As such, initial coordinates for the guest molecules and Brønsted acid site oxygen atoms must be specified. Initial guest molecule coordinates, i.e. reactant and product geometries, for the tautomerization reaction of acetone and subsequent condensation with formaldehyde are taken from previously optimized clusters in our earlier studies of HZSM-5. [29]

As in our previous work [23, 27, 29], the Brønsted acid site in HZSM-5 was chosen to be between Si(2) and Si(8), centered on O(13) (see Fig. 4.2). Due to its proximity to the intersection, O(13) is a catalytically relevant site.[30] We note in Fig. 4.2 the zeolitic oxygen, O(13) is denoted as O1 for ease of numbering adjacent active site oxygens; these are not the crystallographically-sanctioned labels. Using Schrödinger's automated Python API script, delta clusters are carved out of the periodic crystal with respect to the guest molecule and the Brønsted acid site oxygen atoms geometries and then terminated at either Si or O.[31,32] Hydrogen atoms were used to cap terminal Si or O atoms and Si-H bond lengths were set to 1.4 Å., while O-H bond lengths were set to 0.9 Å. In all calculations, terminal –H and –OH groups were frozen in their crystallographic positions.

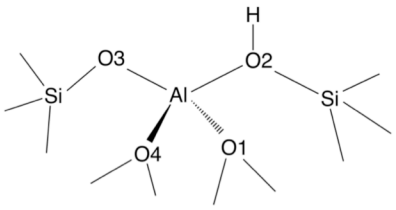

Figure 4.2: Two-dimensional representation of the Brønsted acid site in HZSM-5. We denote the active site oxygens as O1, O2, O3 and O4 for simplicity; these are not the crystallographically-sanctioned labels in HZSM-5, in which the oxygen labeled O1 corresponds to O(13).

4.2.3 Computational Details

The B3LYP[35] hybrid density functional was used with the 6-311G(d,p)[36] basis set as implemented in Gaussian09[34]. Accurate barriers for the acid-catalyzed aldol chemistry have been reported using the same model chemistry.[29] All energies reported are bare potential energies. We have determined the Gibbs energy of activation in selected delta clusters within the harmonic oscillator approximation, and have also implemented dispersion corrections using the Grimme[24] approach as implemented in the electronic structure program Jaguar[38] (see Section 4.3.5); these were not found to influence the reported trends. Atomic charges were calculated using the Merz-Kollman procedure to reproduce the electrostatic potential[39,40].

4.2.3.1 Transition States in Delta Cluster of HZMS-5

Once various sized delta clusters were generated using previously optimized reactant/s and product geometries, initial guesses for transition state geometries were required. In the case of acetone tautomerization, the B3LYP confirmed transition state geometry from our previous work in a 37T cluster of HZSM-5 was used as an initial transition state guess in delta clusters[29]. In a similar fashion, the B3LYP confirmed transition state for the condensation reaction between the enol and formaldehyde, was also taken from our previous work in an 11T cluster of HZSM-5[29].

As in our previous work (see Chapter 2), the semiempirical PM6 approach was used to quickly explore plausible transition state conformations. Before all transition states were located, a constrained optimization was performed, in which atoms involved in the reaction coordinate were frozen, allowing the remaining atoms to relax. In the case

of keto/enol acetone tautomerization, we followed the procedure outlined in our previous computational study[29]. Specifically the acetone carbonyl oxygen, methyl carbon, the two involved protons and the zeolitic O1 and O2 atoms (see Fig. 4.2 for oxygen labels) were frozen at various configurations along a likely reaction coordinate, yielding different initial conditions for full transition state searches. In the case of condensation between the enol and formaldehyde, the constrained optimization involved freezing the coordinates of formaldehyde's carbonyl oxygen, the enol's alcohol group and the two participating carbon and hydrogen atoms at various configurations along the reaction coordinate.

These constrained optimizations were followed by unconstrained transition-state searches. As in our previous work (see Chapter 2), transition states were located using the Berny Optimization algorithm[42], confirmed as first-order saddle points by NMA, and by steepest-descent calculations to confirm that transition states connect with desired reactant and product minima. NMA was performed on all minima to confirm that they are true minima with all real vibrational frequencies. Confirmed transition states were then used as initial transition-state geometries in higher-level calculations using B3LYP/6-311G(d,p). Once the B3LYP transition state was found in a given smaller delta cluster (e.g. δ = 3 Å) and confirmed via NMA following the procedure outlined above, the corresponding transition-state geometry was then used as an initial transition state guess in larger delta clusters of HZSM-5.

4.2.3.2 Locating Transition States for Furfural Condensation in HZSM-5.

Once the transition state for the condensation reaction between the enol and formaldehyde was located in a δ = 4 Å cluster (see Fig. 4.3A), this transition state

geometry and cluster were subsequently used to locate transition states associated with furfural condensation. First, locating the transition state for condensation between the enol and furfural required altering the transition state obtained with formaldehyde condensation. Alteration involved changing a hydrogen atom on formaldehyde into a furan ring. Once the hydrogen was transmuted to form furfural, a constrained optimization was performed at the PM6 level of theory. In the optimization the Brønsted acid site oxygens and all of the atoms in the guest molecule were frozen, except for the furan ring. All other atoms were allowed to relax. Such a constrained optimization allowed the furan ring and zeolite framework to relax with respect to one another. After the constrained optimization, an unconstrained transition state search was performed at the same level of theory. Once located and confirmed via NMA, steepest-descent calculations were employed to obtain the desired reactant and product geometries.

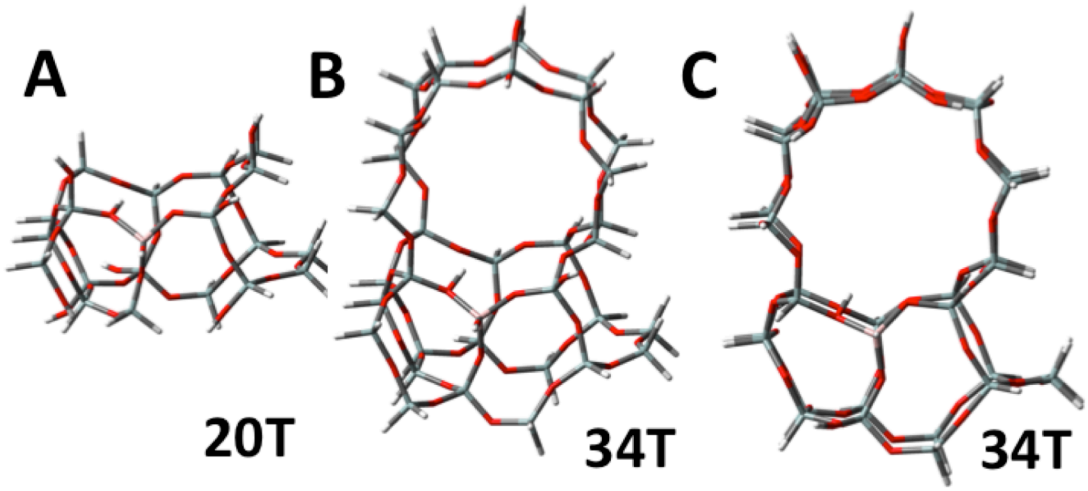

Figure 4.3: Delta clster models of HZSM-5 when δ = 4 Å (shown in tubes) built with respect to the reactant, product and Brønsted acid site oxygen geometries in the aldol condensation reaction between the enol and (A) formaldehyde, (B) furfural and (C) HMF.

Next the reactant, product and zeolitic Brønsted acid site oxygen atom configurations were extracted from the δ = 4 Å cluster, originally built for the condensation reaction with formaldehyde (see Fig. 4.3A). These geometries were then used to build delta clusters of HZSM-5 tailored to model the condensation reaction with furfural (Fig. 4.3B). A δ = 4 Å cluster of HZSM-5, built about the reactant, product and Brønsted acid site oxygen atom geometries, was used to locate the transition state (see Fig. 4.3B). The initial transition state geometry guess was extracted from the B3LYP calculation in the δ = 4 Å cluster, originally built for the condensation reaction with formaldehyde (see Fig. 4.3A). Again constrained optimization in PM6 was performed, followed by unconstrained transition state searches. Once confirmed at the PM6 level, the transition state was then located at the B3LYP level of theory in a δ = 4 Å cluster of HZSM-5 (Fig. 4.3B).

4.2.3.3 Locating Transition States for HMF Condensation in HZSM-5

Once the transition state for the condensation reaction between the enol and furfural was located in a δ = 4 Å cluster (see Fig. 4.3B), the transition state geometry and δ = 4 Å cluster were subsequently used to locate transition states associated with HMF condensation. Similarly to the case of furfural, this first required altering the transition state. Alteration to form HMF involved changing the hydrogen atom adjacent to the furanic oxygen on furfural into a methoxy group (CH_2OH). Once the hydrogen was transmuted to form HMF, a constrained optimization was performed at the PM6 level of theory. Following a similar procedure to that outlined above with furfural, the Brønsted acid site oxygens and all of the atoms in the guest molecule were frozen, except for the methoxy group and the furan ring. All other atoms were allowed to relax. Such a

constrained optimization allowed the furan ring, methoxy group and zeolite framework to relax with respect to one another. After the constrained optimization, a transition state search was performed at the same level of theory. Once located and confirmed via NMA, steepest-descent calculations were employed to obtain the desired reactant and product geometries.

Next reactant, product and zeolitic Brønsted acid site oxygen configurations, were extracted from the $\delta = 4$ Å cluster (see Fig. 4.3B), originally built for the condensation reaction with furfural. These geometries were then used to build delta clusters of HZSM-5 tailored to model the condensation reaction with HMF (Fig. 4.3C). A $\delta = 4$ Å cluster, built about the reactant/product and Brønsted acid site geometries obtained from the above procedure, was used to locate the transition state (Fig. 4.3C). The initial transition state geometry guess was extracted from the B3LYP calculation in the $\delta = 4$ Å cluster, originally built for the condensation reaction with furfural (see Fig. 4.3B). Again constrained optimization in PM6 was performed, followed by unconstrained transition state searches. Once confirmed at the PM6 level, the transition state was then located at the B3LYP level of theory in a $\delta = 4$ Å cluster of HZSM-5 (Fig. 4.3C).

4.3 Results and Discussion

Here we report our results for the aldol condensation reaction catalyzed by HZSM-5 in three main parts. Section 4.3.1, we report the gas phase activation barriers for the mixed aldol condensation for the three reactions. In Section 4.3.2, we discuss the convergence of activation barriers for acetone tautomerization and subsequent condensation with formaldehyde in delta (δ) clusters of HZSM-5. Section 4.3.3 details

barriers and discusses key mechanistic differences for the separate condensation reactions between the acetone enol with furfural and HMF, in $\delta = 4$ Å clusters of HZSM-5.

4.3.1 Gas Phase, Uncatalyzed Aldol Condensations in HZSM-5

The formation of a new carbon-carbon bond in the gas phase mixed aldol condensation occurs in two concerted steps. First keto/enol tautomerization forms the nucleophilic enol. Second the new carbon-carbon bond is built when the enol reacts with an aldehyde. Here we report computed activation barriers for the gas phase aldol condensation between the acetone enol and formaldehyde, furfural and HMF.

Previous studies have shown that the uncatalyzed, gas phase tautomerization is rate-determining in the gas phase aldol condensation reaction with formaldehyde[29]. These studies report tautomerization barriers of ~68 kcal/mol and ~13 kcal/mol for the reaction energy[5, 29]. The gas-phase tautomerization of acetone, having been extensively investigated computationally will not be discussed in detail here. Although the barrier for the gas phase condensation between formaldehyde and the acetone enol was determined to be 15 kcal/mol in our previous work[25] (see Chapter 2), a discussion has been included both for clarity and comparison with barriers associated with furfural and HMF condensation.

Figure 4.4 shows the potential energy diagram for the gas-phase condensation of the acetone enol with formaldehyde, furfural and HMF. Our results for the condensation reaction between the acetone enol and formaldehyde strongly agree with barriers and reaction energies from our previous work (see Chapter 2). The B3LYP/6-311G(d,p) activation energy for condensation between furfural and the acetone enol is 22.3 kcal/mol

and the reaction energy is -9.4 kcal/mol. The activation energy for condensation with HMF is 29.3 kcal/mol and the reaction energy is -2.2 kcal/mol. In Fig. 4.4 the trend between aldehyde size and increasing activation barrier is apparent. As the size of the aldehyde increases, starting from formaldehyde, barriers increase. In Figure 4.4 the gas-phase condensation barrier, for all aldehydes studied, is significantly less than that for tautomerization, consistent with the notion that tautomerization is the rate-determining step in the gas phase.

Moreover the reaction energies become less exothermic, as the size of the aldehyde increases. The trend in increasing endothermicity with aldehyde size is due to the addition of electron donating groups to the carbonyl carbon. In the case of formaldehyde, no electron donating groups are present (see Fig.4.1 I). However in the case of condensation with furfural or HMF an electron donating furan ring is attached to the carbonyl oxygen. Additionally in HMF, a methoxy group attached to the furan ring (see Fig. 4.1 III) is also electron donating. The gas phase reactivities of the aldehydes are directly related to the stablitly that the carbonyl carbon gains from the presence of the electron donating groups. As electron donating groups are added to the carbonyl carbon, more electron density flows into the positively charged carbon, stabilizing the charge and thus decreasing the reactivity of the compound.

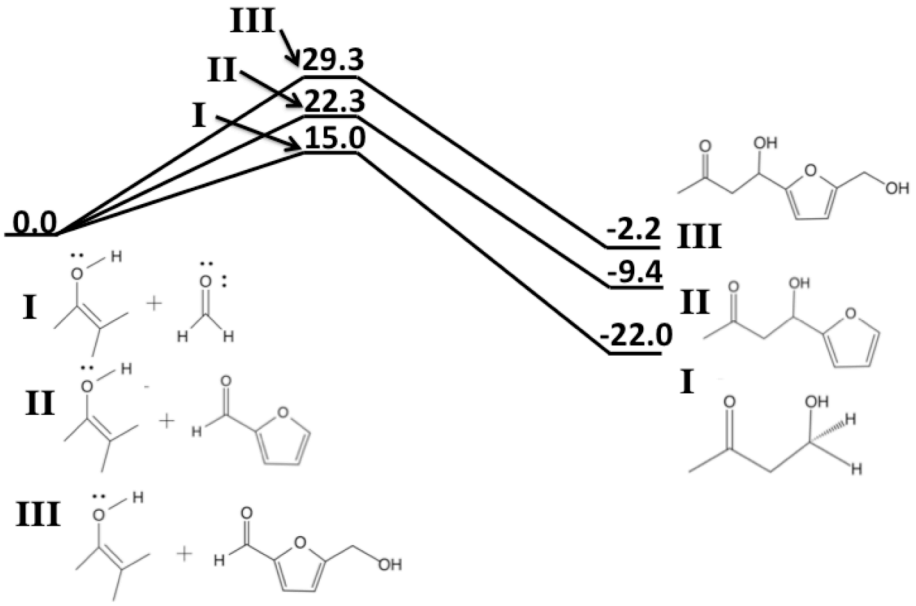

Figure 4.4: Reaction coordinate diagram for the gas-phase, uncatalyzed aldol condensation reactions involving the acetone enol and (I) formaldehyde, (II) furfural and (III) HMF.

4.3.2 Mixed Aldol Condensation Catalyzed in Delta Clusters of HZSM-5

In general, mixed aldol condensation reactions in acid zeolites begin with the adsorption and subsequent tautomerization of acetone at the Brønsted acid site[29]. Once the enol has been formed it has been suggested that condensation proceeds via a concerted mechanism[29]. In the proposed mechanism, adsorption of the aldehyde to the zeolite Brønsted acid site and nucleophilic attack on the aldehyde by the enol occur simultaneously, restoring the carbonyl moiety on the ketone and regenerating the catalytic Brønsted acid site. Here we establish convergence of activation barriers for both keto-enol tautomerization and condensation in delta cluster models of HZSM-5.

The tautomerization of acetone in HZSM-5, having been extensively studied, will be used in the present work to assess the convergence of activation barriers obtained in delta clusters of HZSM-5. Previously computed acetone tautomerization barriers in HZMS-5 of ~20 kcal/mol, obtained in cluster models as large as 37T, serve as a comparison point for our work modeling tautomerization in delta clusters of HZSM-5.[5, 29] Also, the previously studied condensation reaction between tautomerized acetone and formaldehyde is used herein to gauge the accuracy of activation barriers obtained using the delta cluster approach to model aldol condensation.

Figure 4.5A shows the convergence of keto-enol tautomerization activation barriers in various sized delta cluster models of HZMS-5 (see Fig. 4.5B). In delta clusters of HZSM-5, barriers converge to ~20 kcal/mol even at small system sizes- corresponding to small values of δ. Even at small system sizes, the activation barrier agrees strongly with previous computational work that report barriers of ~20.5 kcal/mol. [5, 29]

In Fig. 4.5C we report the convergence of activation barriers for the condensation

reaction between the acetone enol and formaldehyde in various sized delta cluster models of HZMS-5 (see Fig. 4.5D). Figure 4.5C shows that condensation barriers converge to 3.2 kcal/mol at values of $\delta \geq 4$ Å, corresponding to a system size of $\geq$ 20T. The obtained activation energy strongly agrees with the previously reported B3LYP/6-311G(d,p) barrier of 2.0 kcal/mol in a smaller, 11T cluster of HZSM-5[25]. As shown in our previous work (see Chapter 2) this process although strongly catalyzed by HZSM-5, is not rate-determining compared to the barriers associated with acetone tautomerization (~20.5 kcal/mol). We find that in both reaction systems, that a $\delta \geq 4$ Å cutoff is sufficient to converge activation barriers to within chemical accuracy (±1 kcal/mol) in delta clusters of HZSM-5.

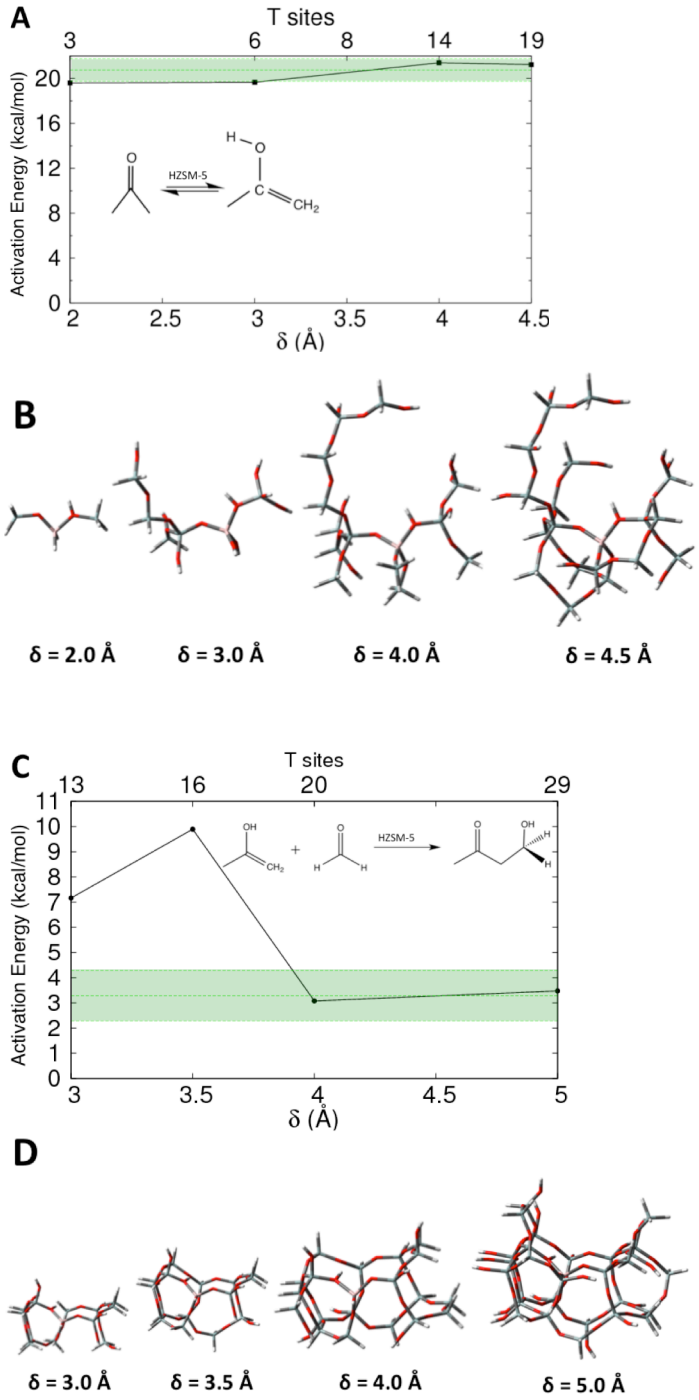

Figure 4.5: The dependence of activation energies for the tautomerization of acetone in delta clusters of HZSM-5 (A). Delta cluster of HZSM-5 constructed about the reactant, product and Brønsted acid site oxygen atom configurations to model keto-enol tautomerization of acetone (B). The dependence of activation barriers for the condensation of formaldehyde with the acetone enol in delta clusters of HZSM-5 (C). Delta cluster of HZSM-5 constructed about the reactant, product and Brønsted acid site oxygen atom configurations to model the condensation reaction between the enol and formaldehyde (D). In both A & B the zone of convergence to within chemical accuracy with respect to system size (± 1 kcal/mol) is shaded in green.

We find that, unlike the case of homogeneous acid catalysis, the condensation mechanism is concerted in HZSM-5. In delta clusters of HZSM-5, we find that formaldehyde activation and carbon-carbon bond formation occur simultaneously. In the homogeneous acid catalyzed mechanism aldehyde activation and carbon carbon bond formation occur in two distinct steps (see Chapter 1, Fig. 1.2). Our results agree with the proposed mechanism in our previous study using a smaller, 11T cluster model of HZSM-5 (see Chapter 2)[29]. However, the condensation mechanism observed in our previous work, involved regenerating the Brønsted acid site at the zeolitic O(1) position in HZSM-5 (see Fig. 4.2 for oxygen labels). In delta clusters of HZSM-5 we find that the condensation mechanism regenerates the Brønsted acid site at the zeolitic O(4) position (see Fig. 4.2 for oxygen labels).

4.3.3 Mixed Aldol Condensation with Furfural catalyzed by HZSM-5

Figure 4.6 shows the potential energy diagram for condensation between the acetone enol and furfural in a δ = 4 Å cluster of HZSM-5. The concerted reaction mechanism, observed in condensation with formaldehyde, is also observed in the case of furfural condensation in HZMS-5. The B3LYP/6-311G(d,p) activation energy for this process is 4.6 kcal/mol with an exothermic reaction energy of -10.5 kcal/mol (see Fig 4.8). While this barrier is significantly lower than the corresponding gas phase reaction (see Fig. 4.4), it is only slightly higher (+1.4 kcal/mol) compared to condensation with formaldehyde in HZSM-5 (Fig. 4.6). As such, acetone tautomerization remains rate-determining in the overall condensation reaction with furfural. In agreement with gas phase trends, the zeolite catalyzed reaction energy for condensation with furfural is more

endothermic compared to that of formaldehyde (Fig. 4.4 and 4.8). However reaction energy differences with respect to the gas phase remain relatively unchanged.

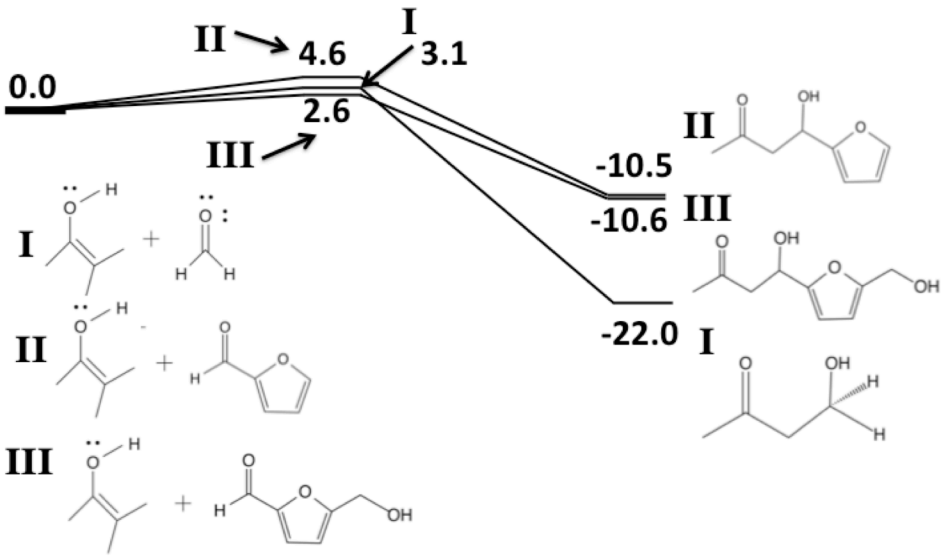

Figure 4.6 Reaction coordinate diagram for the gas-phase aldol condensation reactions involving the acetone enol and (I) formaldehyde, (II) furfural and (III) HMF catalyzed by HZSM-5. All reported energies are obtained in $\delta = 4$ Å clusters of HZSM-5.

At the transition state, all atoms labeled in Fig. 4.7A & B are involved in the imaginary reaction coordinate. Associated with the motion of these eight atoms, are 10 geometric parameters: 8 bond distances and 2 bond angles (see Table 4.1). In order to assess whether the transition state obeys Hammond's postulate or violates it, we have developed a simple approach based on defining a parameter $\lambda = \frac{x-a}{b-a}$, where x = geometric parameter (bond distance or angle) of the transition state geometry , a = geometric parameter (bond distance or angle) of the reactant geometry and b = geometric parameter (bond distance or angle) of the product geometry. If λ is greater than 0.5 the parameter in the transition state is more product-like, whereas if λ is less than 0.5 the parameter in the transition state is more reactant-like. If the transition state and reactant geometries are equivalent, then $\lambda = 0$. If the transition state and product geometries are equivalent, then $\lambda = 1$. We find in the case of condensation between the acetone enol and furfural that only 2 of the parameters yield values of $\lambda > 0.5$ (the C2-C3 bond distance and the O6-H2-O2 bond angle) and that most of the parameters are more reactant-like with values of $\lambda < 0.5$ (see Table 4.1). As such we conclude that the transition state geometry is more like the reactant state geometry than the product geometry, in accordance with Hammond's postulate for an exothermic reaction.

Table 4.1: Reactant, transition state and product geometries for the condensation reaction between furfural and the acetone enol.

Atom Labels	Reactant (a)	Transition State (x)	Product (b)	λ
O3-H1	2.20 Å	1.94 Å	1.57 Å	0.415
H1-O5	0.97 Å	0.98 Å	1.03 Å	0.130
O3-H1-O5	124.2°	134.3°	156.6°	0.312
O5-C1	1.35 Å	1.33 Å	1.26 Å	0.282
C1-C2	1.34 Å	1.36 Å	1.47 Å	0.151
C2-C3	3.59 Å	2.47 Å	1.58 Å	0.555
C3-O6	1.27 Å	1.29 Å	1.40 Å	0.133
O6-H2	1.05 Å	1.02 Å	0.98 Å	0.407
H2-O2	1.49 Å	1.56 Å	1.78 Å	0.233
O6-H2-O2	165.0°	160.8°	157.6°	0.568
Where, $\lambda = \frac{x-a}{b-a}$ If $\lambda > 0.5$ then transition state parameter is more product-like. If $\lambda < 0.5$ then transition state parameter is more reactant-like.				

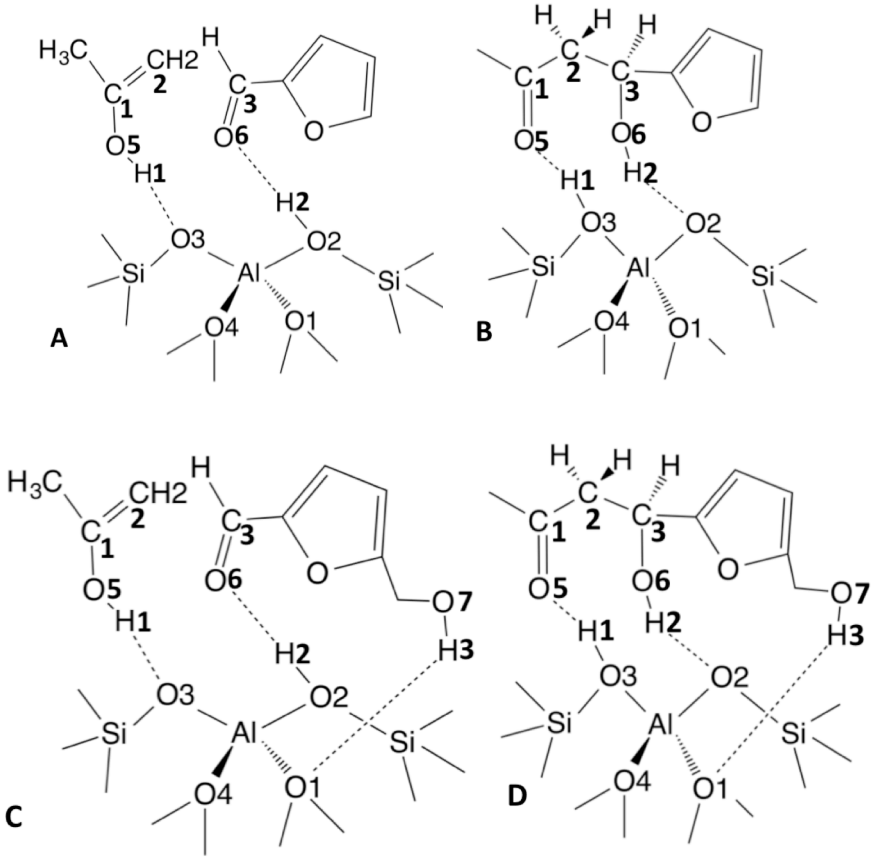

Figure 4.7: Structures for the reactant pair (A) and aldol product (B) from the condensation reaction between furfural and the acetone enol in HZSM-5. Structures for the reactant pair (C) and aldol product (D) from the condensation reaction between HMF and the acetone enol in HZSM-5.

4.3.4 Mixed Aldol Condensation with HMF catalyzed by HZSM-5

Figure 4.6 shows the potential energy diagram for condensation between the acetone enol and HMF in a δ = 4 Å cluster of HZSM-5. The concerted reaction mechanism, observed in condensation with formaldehyde and furfural, is also observed in the case of HMF condensation in HZMS-5. The B3LYP/6-311G(d,p) activation energy for this process is 2.6 kcal/mol with an exothermic reaction energy of -10.6 kcal/mol (see Fig 4.6). This barrier is significantly lower than the corresponding gas phase reaction (see Fig. 4.4), however it is only slightly lower (-1.4 kcal/mol) than the corresponding barrier with furfural in HZSM-5 (Fig. 4.6). Although the barrier is lower than both the gas phase reaction and condensation with formaldehyde or furfural, it is still significantly lower than the barrier for acetone tautomerization (~20.5 kcal/mol) in HZSM-5. As such, acetone tautomerization remains rate-determining in the overall condensation reaction with HMF.

In agreement with the gas phase trends, the zeolite catalyzed reaction energy for condensation with HMF is more endothermic compared to that of formaldehyde (Fig. 4.4 and 4.6). However, unlike the case of furfural condensation, the gas phase trend of increasing endothermicity with increasing reactant size is not recovered for the zeolite-catalyzed condensation of HMF. Counterintuitively, the reaction energy is equivalent to that for furfural condensation (~ -10.5 kcal/mol).

The reaction energies for condensation from our delta cluster models are influenced by attractive interactions with the Brønsted acid site oxygens and the zeolite pore. In the case of furfural condensation the furanic oxygen is significantly further away from the Brønsted acid site oxygen, O1 (see Fig. 4.8 for oxygen labels), compared to the

case of HMF condensation. In condensation with furfural the furanic oxygen and Brønsted acid site oxygen (O1 in Fig. 4.8) are 3.70Å apart. However in condensation with HMF the furanic oxygen and Brønsted acid site oxygen (O1 in Fig. 4.8) are significantly closer to one another at a distance of 2.99Å.

To understand this difference we consider atomic charges. We have computed the Merz-Kollman charges of the reactants in the case of condensation between the acetone enol with furfural or HMF (see Figure 4.8 A & B respectively). Conventional wisdom dictates that the furanic oxygen in both furfural and HMF will be negatively charged. Our calculations reveal that the furanic oxygen in furfural is negatively charged (see Figure 4.8A). Counterintuitively we find that the furanic oxygen in HMF is positively charged (see Figure 4.8B). In the case of condensation with furfural, the negatively charged furanic oxygen repels the guest molecule from the negatively charged acid site oxygen, O1 (Fig.4.8A), and pore wall. However in the condensation reaction with HMF, the opposite occurs and the positively charged furanic oxygen is not repelled but attracted to the negatively charged acid site oxygen, O1 (Fig. 4.8B), and pore wall. The attractive interaction between HMF and the zeolite Brønsted acid site oxygen imparts stabilization to HMF as compared to furfural.

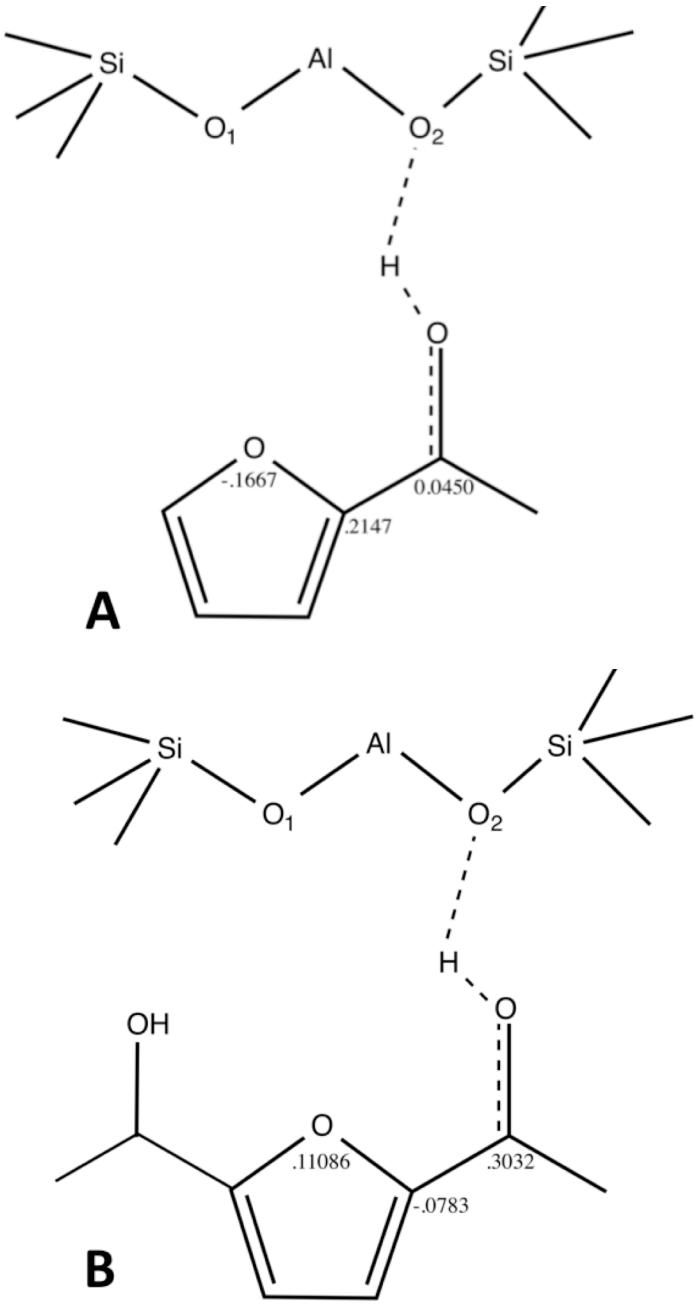

Figure 4.8: Merz-Kollman atomic charges for the aldehydes in the condensation reaction between the acetone enol with furfural or HMF (A) furfural and (B) HMF shown with the Brønsted acid site.

At the transition state all atoms labeled in Fig. 4.7C & D, except for those labeled O7, H3 and O1, are involved in the imaginary reaction coordinate. As in the case of condensation with furfural, associated with the motion of these eight atoms are 10 geometric parameters (see Table 4.2). In section 4.3.3 we defined a parameter, λ, as a simple approach to determine if the transition state obeys Hammond's postulate. We find in the case of condensation between the acetone enol and HMF that only 2 of the geometric parameters yield values of $\lambda > 0.5$ (the C2-C3 distance and the O3-H1-O5 angle). Most of these parameters yield values of $\lambda < 0.5$ and are thus more reactant-like (see Table 4.2). As such we conclude that the transition state geometry in the case of condensation between the acetone enol and HMF is more reactant-like, obeying Hammond's postulate for an exothermic reaction.

Table 4.2: Reactant, transition state and product geometries for the condensation reaction between HMF and the acetone enol.

Atom Labels	Reactant (a)	Transition State (x)	Product (b)	Λ
O3-H1	2.05 Å	1.83 Å	1.51 Å	0.417
H1-O5	0.97 Å	0.98 Å	1.05 Å	0.152
O3-H1-O5	134.0°	146.1	156.8°	0.531
O5-C1	1.35 Å	1.32 Å	1.26 Å	0.309
C1-C2	1.34 Å	1.36 Å	1.47 Å	0.163
C2-C3	3.56 Å	2.44 Å	1.58 Å	0.564
C3-O6	1.28 Å	1.30 Å	1.40 Å	0.144
O6-H2	1.04 Å	1.01 Å	0.98 Å	0.459
H2-O2	1.52 Å	1.60 Å	1.81 Å	0.294
O6-H2-O2	164.0°	158.8	152.8°	0.464
O7-H3	0.97 Å	0.97 Å	0.97 Å	N/A
H3-O1	2.02 Å	2.02 Å	2.09 Å	N/A
O7-H3-O1	155.2°	154.7°	154.3°	N/A

Where, $\lambda = \frac{x-a}{b-a}$
If $\lambda > 0.5$ then transition state parameter is more product-like.
If $\lambda < 0.5$ then transition state parameter is more reactant-like.

4.3.5 Thermodynamic Energy Corrections

All energies reported are bare potential energies. We have determined the Gibbs energy of activation in select delta clusters studied within the harmonic oscillator approximation (Figs. 4.8- 4.9), and have also implemented dispersion corrections (Figs. 4.10- 4.11) using the Grimme[24] approach as implemented in the electronic structure program Jaguar[38]; these were not found to influence the reported trends.

4.3.5.1 Gibbs Corrected Activation Barriers

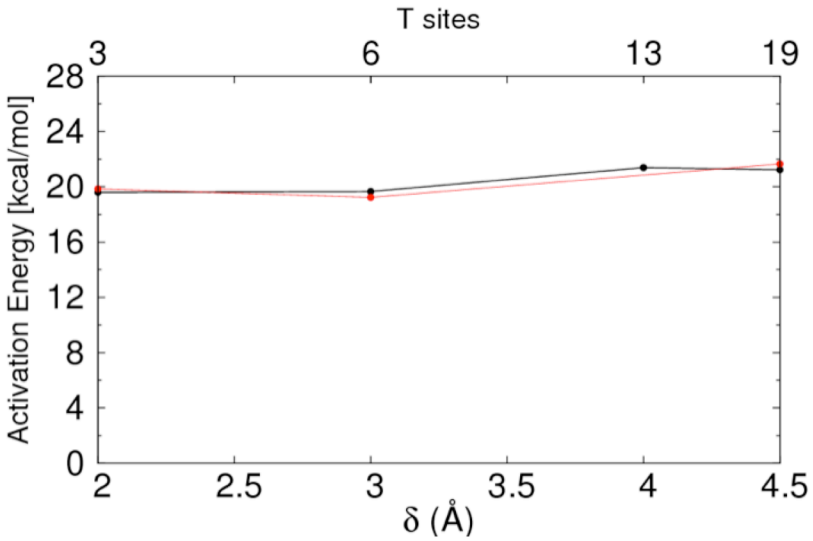

Figure 4.9: Activation energies for the tautomerization of acetone in delta clusters of HZSM-5. Values shown in black correspond to B3LYP/6-311G (d,p) optimized activation energies and those in red correspond to B3LYP/6-311G (d,p) Gibbs activation energies.

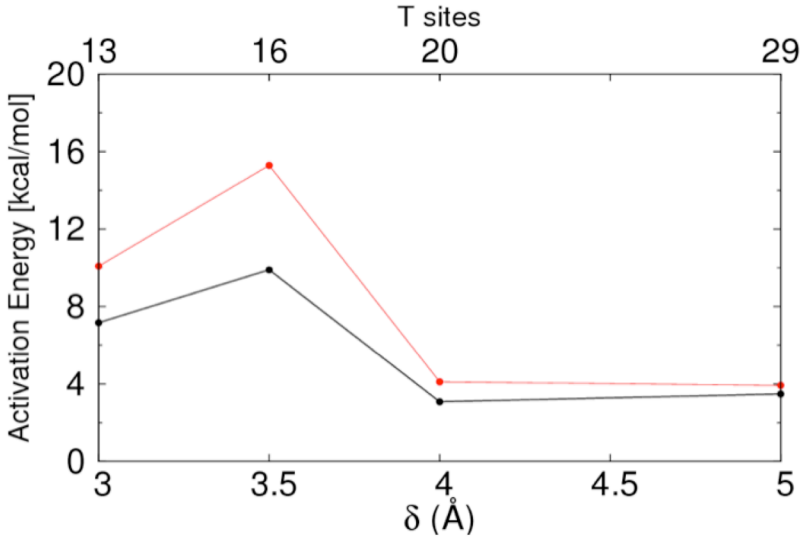

Figure 4.10: Activation energies for the condensation reaction between the acetone enol and formaldehyde in delta clusters of HZSM-5. Values shown in black correspond to B3LYP/6-311G (d,p) optimized activation energies and those in red correspond to B3LYP/6-311G (d,p) Gibbs activation energies.

4.3.5.2 Dispersion Corrected Activation Barriers

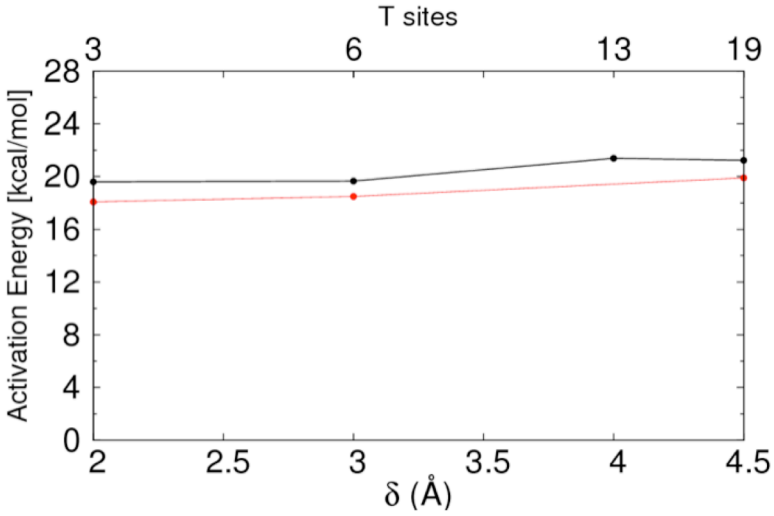

Figure 4.11: Activation energies for the tautomerization of acetone in delta clusters of HZSM-5. Values shown in black correspond to B3LYP/6-311G (d,p) optimized activation energies and those in red correspond to B3LYP/6-311G (d,p) D3 corrected activation energies.

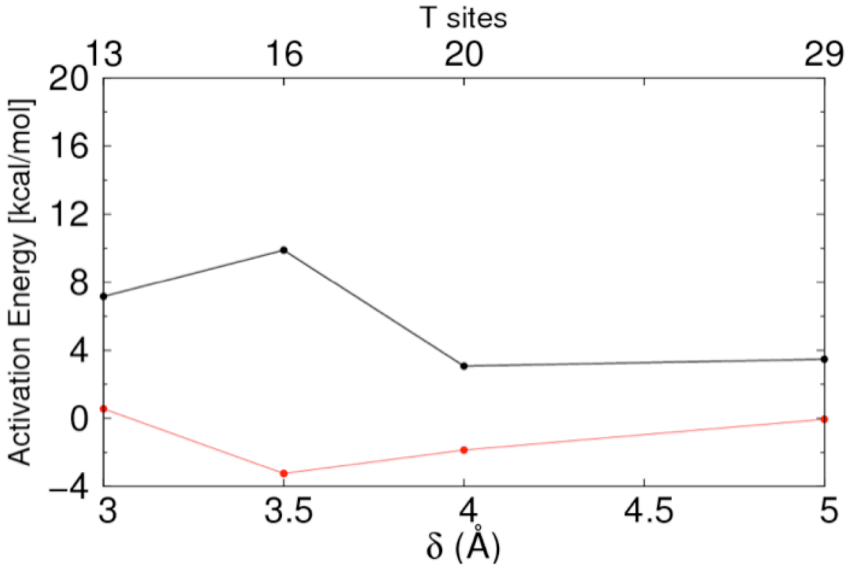

Figure 4.12: Activation energies for the condensation reaction between the acetone enol and formaldehyde in delta clusters of HZSM-5. Values shown in black correspond to B3LYP/6-311G (d,p) optimized activation energies and those in red correspond to B3LYP/6-311G (d,p) D3 corrected activation energies.

4.4 Summary and Concluding Remarks

We have applied DFT calculations to investigate the acid-zeolite-catalyzed mixed aldol condensation of acetone with various aldehydes in delta clusters of HZSM-5. We have used two reactions, relevant to biomass conversion, as platforms to establish convergence of activation barriers using delta clusters. First, we have examined the unimolecular tautomerization reaction of acetone, the rate-determining step in condensation, and second the bimolecular condensation between the enol and formaldehyde, in which a new carbon-carbon bond is built. We find that in both reaction systems, that a $\delta \geq 4$ Å cutoff is sufficient to converge activation barriers to within chemical accuracy (±1 kcal/mol) in delta clusters of HZSM-5.

We have modeled the aldol condensation between the enol and more relevant biomass-derived aldehydes, furfural and HMF, in $\delta = 4$ Å (~34T) cluster models of HZSM-5. We report barriers for condensation between the enol and furfural or hydroxymethylfurfural as 4.6 kcal/mol and 2.6 kcal/mol, respectively. We conclude that the keto/enol tautomerization of acetone remains rate-determining even in the case of condensation with furfural or hydroxymethylfurfural. We have discovered that unlike the case of homogeneous acid catalysis, the mechanism for the condensation step in HZSM-5 is concerted. We find that aldehyde activation and carbon-carbon bond formation occur simultaneously in HZSM-5. Moreover, in delta clusters of HZSM-5 we find that the Brønsted acid site is regenerated at the zeolitic O(4) position, instead of the zeolitic O(1) position of the previously proposed mechanism in an 11T cluster of HZSM-5.

We have used a simple method to analyze the geometrical parameters involved in the imaginary reaction coordinate for the reactant, product and transition state in the

condensation reaction. We have concluded, from our analysis, that the transition state geometry is closer to the reactant state geometry than to that of the product. As such, we find that the exothermic condensation reaction between the acetone enol and either furfural or HMF obeys Hammond's postulate and that the transition state occurs early in the reaction.

CHAPTER 5
CONCLUSIONS AND SUGGESTIONS FOR FUTURE WORK

5.1. Conclusions

5.1.1 Mixed Aldol Condensation catalyzed by HZSM-5 and HY

We applied DFT to investigate the mixed aldol condensation of acetone and formaldehyde in acid zeolites HZSM-5 and HY, as a prototypical bond-forming reaction in biofuel production. We modeled the acid-catalyzed reaction in HZSM-5 and HY in two steps: keto/enol tautomerization of acetone, and bimolecular condensation between formaldehyde and the acetone enol. For both acid zeolites, the keto/enol tautomerization of acetone was found to be the rate-determining step, consistent with the accepted mechanism in homogeneous acid-catalysis. Convergence studies of the activation energy for keto/enol tautomerization, with respect to cluster sizes of HZSM-5 and HY, exhibit rather different convergence properties for the two zeolites. The keto/enol activation energy was found to converge in HY to ~20 kcal/mol for a cluster with 11 tetrahedral atoms (11T cluster), which does not complete the HY supercage. In contrast, the activation energy for HZSM-5 reaches an initial plateau at a value of ~28 kcal/mol for clusters smaller than 20T, and then converges to ~20 kcal/mol for clusters of size 26T or greater, well beyond the completion of the HZSM-5 pore. As such, completing a zeolite pore surrounding a Brønsted acid site may be insufficient to converge activation energies; instead, we recommend an approach based on converging active-site charge.

5.1.2 Rational Design of Zeolite Clusters

We have applied DFT calculations to systematically investigate zeolite cluster-size convergence for two acid-zeolite-catalyzed processes related to the conversion of biomass: (1) the keto-enol tautomerization of acetone in HZSM-5 and HY, and (2) the protonation and ring opening of furan in HZSM-5. We have used these reactions as platforms to study two different approaches for constructing successively larger cluster models of zeolites, with the aim of determining a protocol that converges the energy differences with minimal system size. One approach for cluster design involves counting framework bonds from the Brønsted acid-site aluminum atom. Another approach involves applying multi-centered spherical cutoffs based on geometries of the zeolite active site, the adsorbed reactant, and the adsorbed product. We have investigated the convergence of reaction energies using single-point calculations on clusters containing as many as 166 tetrahedral (T) atoms, and geometry optimizations on clusters with as many as 78 T-atoms. For all reactions studied, convergence rates of single-point reaction energies agree well with those from geometry-optimized clusters. In addition, converged and optimized reaction energies agree well with previously published values for all reactions. Our central finding is that clusters generated with multi-centered spherical cutoffs yield converged reaction energies with smaller system sizes than clusters generated by counting framework bonds. This method, employing a single length scale (5 Å), converges reaction energies with respect to system size to within chemical accuracy (±1 kcal/mol), and includes between 15 and 34 T-atoms in the cluster depending on the process and zeolite framework under investigation. We suggest a general protocol for

generating such clusters for subsequent use in computational studies of zeolites and other heterogeneous catalysts.

5.1.3 Mixed Aldol Condensation Reactions Catalyzed by HZSM-5

We have applied DFT calculations to investigate the acid-zeolite-catalyzed mixed aldol condensation of acetone with various aldehydes in delta clusters of HZSM-5. We have used two reactions, relevant to biomass conversion, as platforms to establish convergence of activation barriers using delta clusters. We find that in both reaction systems, that a $\delta \geq 4$ Å cutoff is sufficient to converge activation barriers to within chemical accuracy (±1 kcal/mol) in delta clusters of HZSM-5.

We have modeled the aldol condensation between the enol and more relevant biomass-derived aldehydes, furfural and hydroxymethylfurfural (HMF), in $\delta = 4$ Å (~34T) cluster models of HZSM-5. We have discovered that unlike the case of homogeneous acid catalysis, the mechanism for the condensation step in HZSM-5 is concerted. We report barriers for condensation between the enol and furfural or hydroxymethylfurfural as 4.6 kcal/mol and 2.6 kcal/mol, respectively. We conclude that the keto/enol tautomerization of acetone remains rate-determining even in the case of condensation with furfural or hydroxymethylfurfural.

5.2 Suggestions for Future Work

A central finding of our work, presented in Chapters 2 and 4, has been that the keto-enol tautomerization of acetone is rate-determining in the mixed aldol condensation reaction in HZSM-5 and HY, with a activation barriers of ~20 kcal/mol for

both zeolites. Given that HZSM-5 and HY are strong Brønsted acids, it is unlikely that the barrier for tautomerization would be lower in another zeolite framework with similar Brønsted acidity. Since zeolites are known to exhibit Lewis acid properties, a clear extension of our work would be to study the rate-determining, keto-enol tautomerization of acetone catalyzed by zeolites possessing strong Lewis acid sites. We hypothesize that the presence of a Lewis acid will change the reaction mechanism associated with the tautomerization of acetone. Such an alternative could provide a reaction path, in which the barrier to form the reactive enol could be significantly lower than that of HZSM-5. As such, future work should address the following key questions:

- How do zeolites with Lewis Acid sites catalyze keto-enol tautomerization reactions?
- How does the mechanism change?
- What role does the Lewis Acid play in catalysis?

In order to investigate possible reaction mechanisms for acetone tautomerizaion in Sn-substituted ZSM-5, viable guesses as to the geometry of the active site and the transition state must first be generated. In Figures 5.1 and 5.2, two plausible reaction pathways are suggested for future study. The proposed mechanism in Figure 5.1 is based on the concerted, uncatalyzed gas phase reaction mechanism (see Fig. 2.3), in which acetone self-donates a proton from a methyl group to the carbonyl oxygen to form the enol. It is hypothesized that the mechanism in Sn-substituted ZSM-5 could be similar to that of the uncatalyzed, gas phase reaction and that the compound's interaction with Sn will facilitate more facile proton transfer (from the methyl on acetone to the carbonyl carbon).

A non-concerted mechanism is proposed in Figure 5.2. In this mechanism a defect must be first be introduced into the zeolite framework (see Fig 5.2A, B & C), by deprotonation of the methyl group by an active site oxygen. Preliminary calculations suggest that protonation of an active site oxygen could break the Sn-O bond (see Fig. 5.2C). Once the –OH group has been formed on the acid site oxygen, the hydrogen can then transfer to the carbonyl oxygen and form the enol. Although this mechanism is not concerted and involves two transition states and an intermediate, the barriers associated with each step could be lower than the barrier associated with tautomerization in HZSM-5. Lowering the barrier associated with acetone tautomerization would represent a significant step in biofuel refinement.

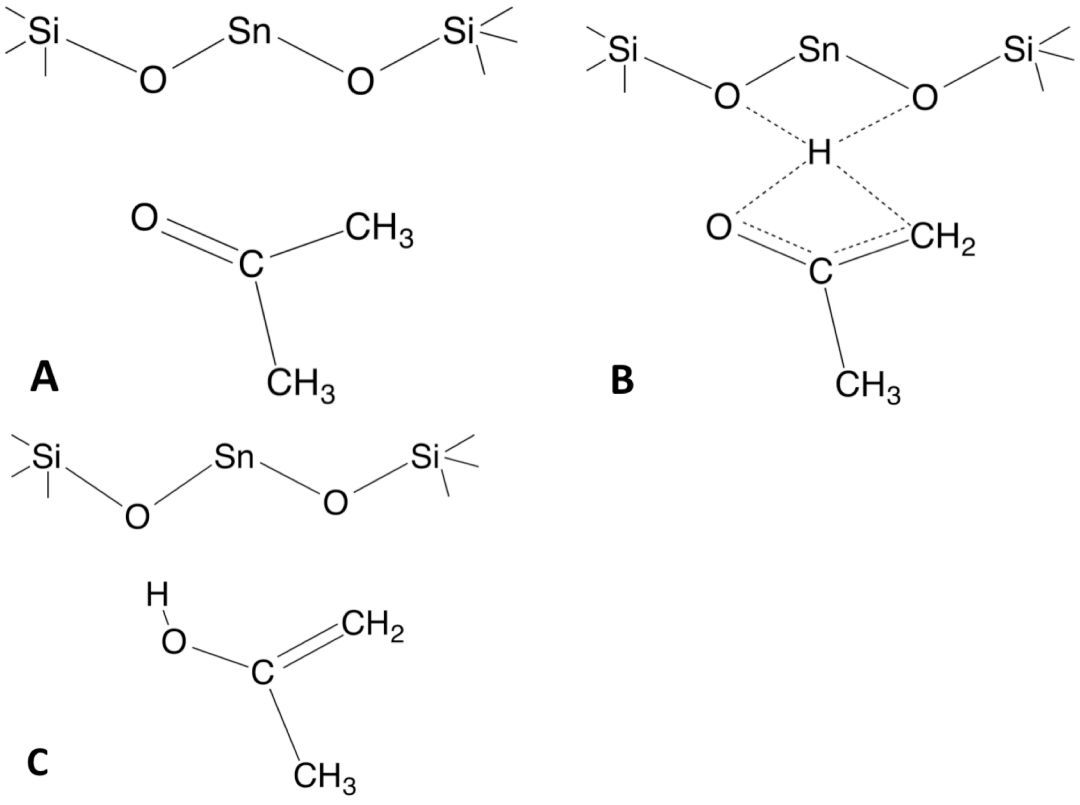

Figure 5.1: Proposed mechanism for the tautomerization of acetone in Sn-substituted HZSM-5. Reactant state (acetone) , transition state and product
state (acetone enol) are shown in A, B, C respectively.

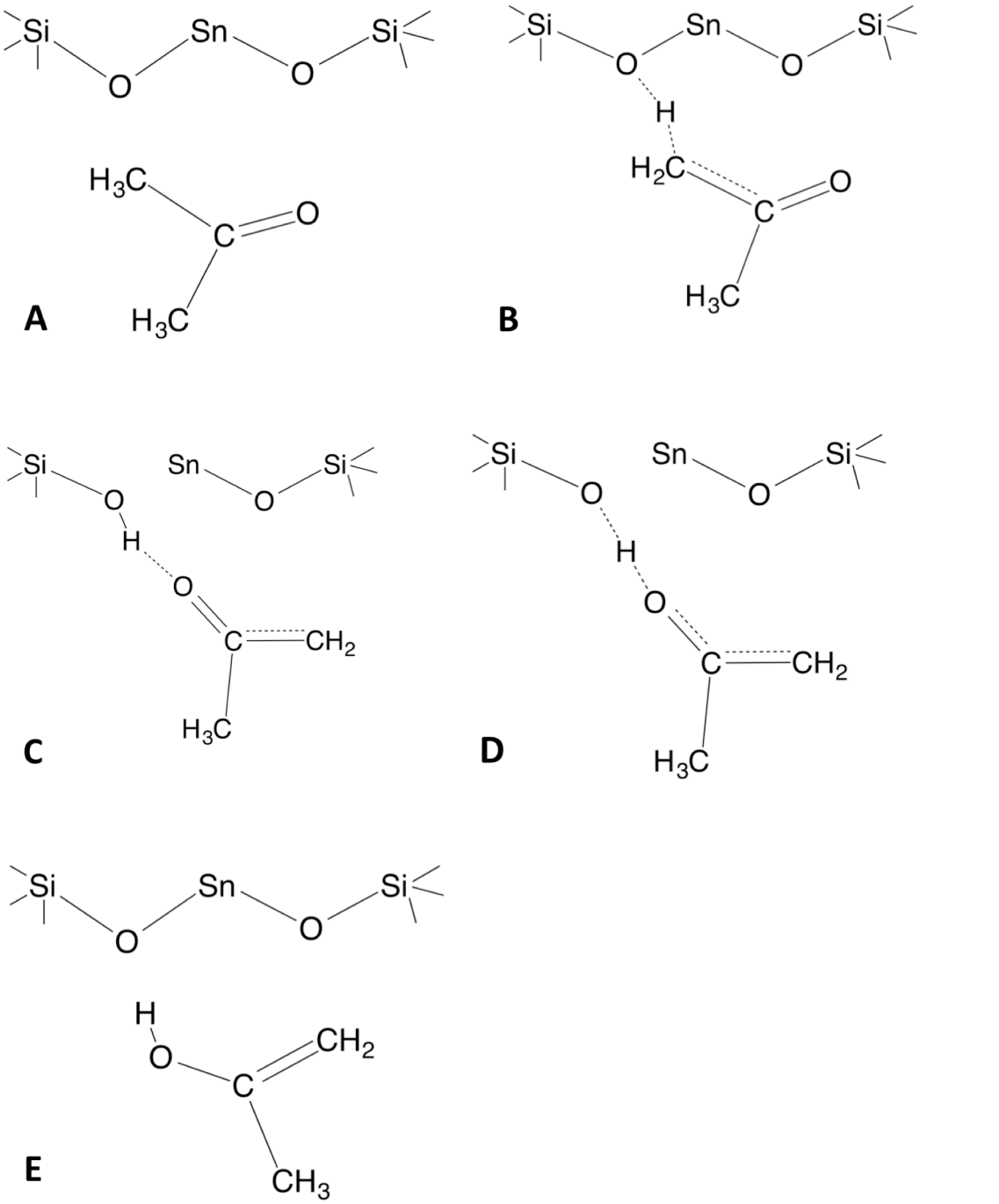

Figure 5.2: Proposed reaction mechanism for the tautomerization of acetone in Sn-substituted HZSM-5. Reactant state (acetone), intermediate state and product state (acetone enol) are shown in A , C & E respectively. Transition states 1 and 2 are shown in B & D, respectively.

BIBLIOGRAPHY

1. Lu, Q.; Zhang, X. M.; Zhang, Z. B.; Zhang, Y.; Zhu, X. F.; C.Q., D. Catalytic Fast Pyrolysis of Cellulose Mixed with Sulfated Titania to Produce Levoglucosenone: Analytical Py-GC/MS study. *BioRes.* **2012,** *7* (3), 2820-2834.

2. Xie, H.; Gathergood, N. *The Role of Green Chemistry in Biomass Procesing and Conversion.* John Wiley and Sons: Hoboken, NJ, 2013.

3. A.V., S.; S., T.; G.W., H. C-C Bond Formation Reactions for Biomass-Derived Molecules. *ChemSusChem* **2010,** *10* (3), 1158-1161.

4. Resasco, D. E.; Sitthisa, S.; Faria, J.; Prasomsri, T.; Pilar Ruiz, M. Furfurals as Chemical Platform for Biofuels Production. In *Heterogeneous Catalysis in Biomass to Chemicals and Fuels*, Kubička, D.; Kubicoková, I., Eds. Research Signpost: 2012.

5. Boekfa, B.; P., P.; Probst, M.; J., L. Adsorption and Tautomerization Reaction of Acetone on Acidic Zeolites: The Confinement Effect in Different Types of Zeolites. *J. Phys. Chem. C.* **2010,** *114*, 15061-15067.

6. Solans-Monfort, X.; J., B.; Branchadell, V.; Sodupe, M. J. Keto-Enol Isomerization of Acetaldehyde in HZSM5. A Theoretical Study Using the ONIOM2 Method. *J. Phys. Chem. B.* **2002,** *106*, 10220-10226.

7. Speybroeck, V. V.; Mynsbrugge, J. V. d.; Vandichel, M.; Hemelsoet, K.; Lesthaeghe, D.; Ghysels, A.; G.B., M.; M., W. First Principle Kinetic Studies of Zeolite-catalyzed Methylation Reactions. *J. Amer. Chem. Soc.* **2011,** *133*, 888-899.

8. W., S.; G.A., T.; K.D., H.; R., X.; F., D.; C.P., G.; Conner Jr., W. C.; Auerbach, S. M.; Huber, G. W. Liquid Phase Aldol Condensation Reactions with MgO-ZrO2 and Shape-Selective Nitrogen-Substituted NaY. *App. Catal. A: General* **2011,** *392*, 57-68.

9. Davis, R. J. New Perspectives on Basic Zeolites as Catalysts and Catalyst Supports. . *Journal of Catalysis* **2003,** *216*, 396-405.

10. Jungho, J.; Tompsett, G. A.; Foster, A. J.; Hammond, K. D.; Auerbach, S. M.; Lobo, R. F.; Huber, G. W. Investigation into the Shape Selectivity of Zeolite Catalysts for Biomass Conversion. *Journal of Catalysis* **2011,** *257*, 257-268.

11. Auerbach, S. M.; Carrado, K. A.; Dutta, P. K. *Handbook of Zeolite Science and Technology*. Dekker: New York, NY, 2003.

12. Weitkamp, J. Zeolites and Catalysis,. *Solid State Ionics* **2000,** *131*.

13. Sastre, G.; Corma, A. The Confinement Effect in Zeolites. *J. Mol.Catal. A: Chem.* **2009,** *305* (1-2), 3-7.

14. Kresse, G.; Hafner, J. Ab initio molecular dynamics for liquid metals. *Phys. Rev. B* **1993,** *47* (:558).

15. Astala, R.; Auerbach, S. M.; Monson, P. A. Density Functional Theory Study of Silica Zeolite Structures: Stabilities and Mechanical Properties of SOD, LTA, CHA, MOR, and MFI. *J. Phys. Chem. B.* **2004,** *108*, 9208-9215.

16. Astala, R.; Auerbach, S. M. The Properties of Methylene- and Amine-Substituted Zeolites from First Principles. *Journal of the American Chemical Society* **2004,,** *126*, 1843-1848.

17. Astala, R.; Auerbach, S. M.; Monson, P. A. Normal Mode Approach for Predicting the Mechanical Properties of Solids from First Principles: Application to Compressibility and Thermal Expansion of Zeolites. *Phys. Rev. B* **2005,** *71*, 14112-14127.

18. Baerlocher, C.; Meier, W. M.; Olson, D. H. *Atlas of Zeolite Framework Types*. 5 ed.; Amsterdam: The Netherlands, 2001.

19. Brändle, M.; Sauer, J. Combining Ab initio Techniques with Analytical Potential Functions. A Study of Zeolite-Adsorbate Interactions of NH3 on H-Faujasite. *J. Mol. Catal. A Chemical* **1997,** *119*, 19-33.

20. Tuma, C.; Sauer, J. Treating Dispersion Effects in Extended Systems by Hybrid MP2:DFT Calculations - Protonation of Isobutene in Zeolite Ferrierite. *Physical Chemistry Chemical Physics* **2006,** *8*, 3955-3965.

21. Moor, B. A. D.; Reyniers, M.-F.; Sierka, M.; Sauer, J.; Marin, G. B.; . Physisorption and Chemisorption of Hydrocarbons in H-FAU Using QM-Pot(MP2//B3LYP) Calculations. *J. Phys. Chem. C* **2008,** *112,* , 11796-11812.

22. Eichler, U.; Kolmel, C. M.; Sauer, J. Combining ab initio techniques with analytical potential functions for structure predictions of large systems: Method and application to crystalline silica polymorphs. *Journal of Computational Chemistry* **1997,** *18*, 463-477.

23. Agarwal, V.; Huber, G. W.; Conner Jr., W. C.; Auerbach, S. M. DFT Study of Nitrided Zeolites: Mechanism of Nitrogen Substitution in HY and Silicalite. *Journal of Catalysis* **2010,** *270*, 249-255.

24. Maihom, T.; Pantu, P.; Tachakritikul, C.; Probst, M.; Limtrakul, J. Effect of the Zeolite Nanocavity on the Reaction Mechanism of n-Hexane Cracking: A Density Functional Theory Study. *J. Phys. Chem. C* **2010,** *114*, 7850-7856.

25. Namuangruk, S.; Pantu, P.; Limtrakul, J. Alkylation of benzene with ethylene over faujasite zeolite investigated by the ONIOM method. *Journal of Catalysis* **2004,** *225*, 523-530.

26. Gomes, J.; Zimmerman, P. M.; Head-Gordon, M.; Bell, A. T. Accurate Prediction of Hydrocarbon Interactions with Zeolites Utilizing Improved Exchange-Correlation Functionals and QM/MM Methods: Benchmark Calculations of Adsorption Enthalpies and Application to Ethene Methylation by Methanol. *J. Phys. Chem. C.* **2012,** *116*, 15406-15414.

27. Vaitheeswaran, S.; Green, S. K.; Dauenhauer, P.; Auerbach, S. M. On the Way to Biofuels from Furan: Discriminating Diels–Alder and Ring-Opening Mechanisms. *ACS Catal* **2013,** *3* (9), 2012-2019.

28. Bao, X. Y.; Sung, C. Y.; Snurr, R. Q.; Broadbelt, L. J. The rate-determining step in the NOx reduction mechanism on BaY zeolites and the importance of long-range lattice effects. *ACS Catal.* **2012,** *2* 350-359.

29. Migues, A. N.; Vaitheeswaran, S.; Auerbach, S. M. Density Functional Theory Study of Mixed Aldol Condensation Catalyzed by Acidic Zeolites HZSM-5 and HY. *Journal of Physical Chemistry C* **2014,** *118* (35), 20283-20290.

30. Fermann, J. T.; Moniz, T.; Kiowski, O.; McIntire, T. J.; Auerbach, S. M.; Vreven, T.; Frisch, M. J. Modeling Proton Transfer in Zeolites: Convergence Behavior of Embedded and Constrained Cluster Calculations. . *J. Chem. Theory Comput.* **2005,** (1), 1232-1239.

31. Czjzek, M.; Jobic, H.; Fitch, A. N.; T., V. Direct Determination of Proton Positions in DY and HY Zeolite Samples by Neutron Powder Diffraction. *J. Phys. Chem. C* **1992,** *96* (4), 1535-1540.

32. van Koningsveld, H.; Jansen, J. C.; van Bekkum, H. The Monoclinic Framework Structure of Zeolite H-ZSM-5. Comparison with the Orthorhombic Framework of As-synthesized ZSM-5. . *Zeolites* **1990,** *10*, 235-242.

33. Schrödinger, L. *Maestro*, 9.4; New York, NY, 2013.

34. Frisch, M. J.; Trucks, G. W.; Schlegel, H. B.; Scuseria, G. E.; Robb, M. A.; Cheeseman, J. R.; Scalmani, G.; Barone, V.; Mennucci, B.; Petersson, G. A. *Gaussian 09, Revision B.01*, Gaussian, Inc.: Wallingford, CT, 2009

35. Becke, A. D. Density-functional Thermochemistry. III. The Role of Exact Exchange. *Journal of Chemical Physics* **1993,** *98* (7), 5648-5652.

36. Krishnan, R.; Binkley, J. S.; Seeger, R.; Pople, J. A. Self-Consistent Molecular Orbital Methods. XX. A Basis Set for Correlated Wavefunctions. *Journal of Chemical Physics* **1980,** *72*, 650.

37. Grimme, S. Semiempirical GGA-type Density Functional Constructed with a Long-range Dispersion Correction. *J. Comp. Chem.* **2006,** *27*, 1787-1799.

38. Bochevarov, A. D.; Harder, E.; Hughes, T. F.; Greenwood, J. R.; Braden, D. A.; Philipp, D. M.; Rinaldo, D.; Halls, M. D.; Zhang, J.; Friesner, R. A. Jaguar: A High-Performance Quantum Chemistry Software Program with Strengths in Life and Materials. *Int. J. Quantum Chem.* **2013,** *113* (18), 2110−2142.

39. Singh, U. C.; Kollman, P. A. An Approach to Computing Electrostatic Charges for Molecules. *J. Comp. Chem.* **1984,** *5*, 129-145.

40. Besler, B. H.; Merz Jr., K. M.; Kollman, P. A. Atomic Charges Derived from Semiempirical Methods. *J. Comp. Chem.* **1990,** *11*, 431-439.

41. Stewart, J. J. P. Optimization of parameters for semiempirical methods. V. Modification of NDDO approximations and application to 70 elements. *Journal of Molecular Modeling* **2007,** *13*, 1173-1213.

42. Schlegel, H. B. Optimization of Equilibrium Geometries and Transition Structures. *J. Comp. Chem.* **1982,** *3*, 214-218.

43. Csicsery, S. M. Acid Catalyzed Isomerization of Dialkylbenzenes. *Journal of Organic Chemistry* **1969,** *34* (11), 3338-3342.

44. Dessaue, R. M. Shape-selective Reactions of Zeolites – Selective Metal-catalyzed Hydrogenation and Oxidations Using ZSM-5. *Journal of Catalysis* **1982,** *77* (1), 304-306.

45. Holmes, J. L.; Lossing, F. P. Heats of Formation of the Ionic and Neutral Enols of Acetaldehyde and Acetone. *Journal of the American Chemical Society* **1982,** *104*, 2648-2649.

46. Turecek, F.; Havlas, Z. Thermochemistry of Unstable Enols: The O-(Cd)(H) Group Equivalent. *Journal of Organic Chemistry* **1986,** *51*, 4066-4067.

47. Zhao, Y.; Truhlar, D. G. Density Functionals with Broad Applicability in Chemistry. *Accounts of Chemical Research* **2008,** *41*, 157.

48. Zhao, Y.; Truhlar, D. G. The M06 Suite of Density Functionals for Main Group Thermochemistry, Kinetics, Noncovalent Interactions, Excited States, and Transition Elements: Two New Functionals and Systematic Testing of Four M06 Functionals and Twelve Other Functionals. . *Theoretical Chemistry Accounts* **2008,** *120*, 215-241.

49. Cheng, Y.-T.; Huber, G. W. Chemistry of furan conversion into aromatics and olefins over HZSM-5: a model biomass conversion reaction. *ACS Catal* **2011,** *1*, 611−628.

50. Cheng, Y.-T.; Jae, J.; Shi, J.; Fan, W.; Huber, G. W. Production of Renewable Aromatic Compounds by Catalytic Fast Pyrolysis of Lignocellulosic Biomass with Bifunctional Ga/ZSM-5 Catalysts. *Angew. Chem., Int. Ed.* **2012,** *51*, 1387−1390.

51. Migues, A. N.; Muskat, A.; Auerbach, S. M.; Sherman, W.; S, V. On the Rational Design of Zeolite Clusters. *ACS Catal.* **2015,** *5* (5), 2859-2865.

52. Tabasso, S.; Cravotto, G. Platform Chemicals from Biomass Using Microwave Irradiation. In *Production of Biofuels and Chemicals with Microwave*, Fang, Z.; Smith, J., R.L. ; Qi, X., Eds. Springer Science + Businees Media Dordrecht, 2015; p 132.